Article

The developing bird pelvis passes through ancestral dinosaurian conditions

https://doi.org/10.1038/s41586-022-04982-w

Received: 8 July 2021

Accepted: 15 June 2022

Published online: 27 July 2022

Check for updates

Christopher T. Griffin[1,2,3], João F. Botelho[1,2,4], Michael Hanson[1,2], Matteo Fabbri[1,2,5], Daniel Smith-Paredes[1,2], Ryan M. Carney[6], Mark A. Norell[7], Shiro Egawa[8], Stephen M. Gatesy[9], Timothy B. Rowe[10], Ruth M. Elsey[11], Sterling J. Nesbitt[3] & Bhart-Anjan S. Bhullar[1,2] ✉

Living birds (Aves) have bodies substantially modified from the ancestral reptilian condition. The avian pelvis in particular experienced major changes during the transition from early archosaurs to living birds[1,2]. This stepwise transformation is well documented by an excellent fossil record[2–4]; however, the ontogenetic alterations that underly it are less well understood. We used embryological imaging techniques to examine the morphogenesis of avian pelvic tissues in three dimensions, allowing direct comparison with the fossil record. Many ancestral dinosaurian features[2] (for example, a forward-facing pubis, short ilium and pubic 'boot') are transiently present in the early morphogenesis of birds and arrive at their typical 'avian' form after transitioning through a prenatal developmental sequence that mirrors the phylogenetic sequence of character acquisition. We demonstrate quantitatively that avian pelvic ontogeny parallels the non-avian dinosaur-to-bird transition and provide evidence for phenotypic covariance within the pelvis that is conserved across Archosauria. The presence of ancestral states in avian embryos may stem from this conserved covariant relationship. In sum, our data provide evidence that the avian pelvis, whose early development has been little studied[5–7], evolved through terminal addition—a mechanism[8–10] whereby new apomorphic states are added to the end of a developmental sequence, resulting in expression[8,11] of ancestral character states earlier in that sequence. The phenotypic integration we detected suggests a previously unrecognized mechanism for terminal addition and hints that retention of ancestral states in development is common during evolutionary transitions.

Birds (Aves) display a dizzying array of ecologies and a radically divergent body plan relative to other vertebrates. Nearly every aspect of avian morphology has been heavily modified from the ancestral archosaurian condition: the avian integument is covered in complex feathers[12,13], the brain and eyes have expanded[14,15], the rostrum has transformed into a beak[16,17], the skeleton is lightweight and pneumatic[18], and the forelimbs have been modified into powerful wings[19]. Like the pectoral region, the avian pelvis underwent a radical transformation during the transition from the ancestral archosaurian configuration to that of birds (Fig. 1). The ilium was greatly extended both posteriorly and anteriorly, and the hip socket (acetabulum) became perforated. The avian pubis is retroverted to face backwards, whereas in most other tetrapods, including in many non-avian dinosaurs, it faces anteriorly. Unlike those of most archosaurs, the distal ends of the pubes are not fused to each other (the pubic symphysis is open[20]). In concert to these pelvic changes, the ancestrally large, muscular tail has been reduced to a shortened pygostyle. All of these transformations (Fig. 1) are associated with the uniquely avian mode of bipedal locomotion in which the femur is largely horizontal and stationary and the lower leg swings to produce motive force[1,20–24]. The sequence of anatomical changes during the origin of the avian pelvis is now well constrained by an excellent fossil record[2–4] (Fig. 1). Many key alterations first appeared in non-avian dinosaurs[25]; indeed, the bird-like characteristics of the dinosaurian pelvis were quickly recognized in the nineteenth century[26,27]. Evolutionary changes morphology are intimately linked to shifts in developmental patterns[28], but information on the evolution of avian pelvic development is lacking (see historical review in the Supplementary Information), especially with regard to early organogenesis and integration of the skeletal, muscular and nervous tissues[29,30].

Major morphological changes may evolve through changes in early developmental events[31] or, at the other extreme, by late modification through terminal addition[8,9]. However, the prevalence of terminal addition in general as a mechanism for the evolution of morphological novelty among deep (that is, 'class'-level) divergences has been much debated[8–11].

[1]Department of Earth and Planetary Sciences, Yale University, New Haven, CT, USA. [2]Yale Peabody Museum of Natural History, Yale University, New Haven, CT, USA. [3]Department of Geosciences, Virginia Tech, Blacksburg, VA, USA. [4]Departamento Biología Celular y Molecular, Pontificia Universidad Católica de Chile, Santiago, Chile. [5]Nagaunee Integrative Research Center, Field Museum of Natural History, Chicago, IL, USA. [6]Department of Integrative Biology, University of South Florida, Tampa, FL, USA. [7]Division of Vertebrate Paleontology, American Museum of Natural History, New York, NY, USA. [8]RIKEN Center for Biosystems Dynamics Research, Kobe, Japan. [9]Department of Ecology and Evolutionary Biology, Brown University, Providence, RI, USA. [10]Jackson School of Geosciences, The University of Texas at Austin, Austin, TX, USA. [11]Rockefeller Wildlife Refuge, Louisiana Department of Wildlife and Fisheries, Grand Chenier, LA, USA. ✉e-mail: bhart-anjan.bhullar@yale.edu

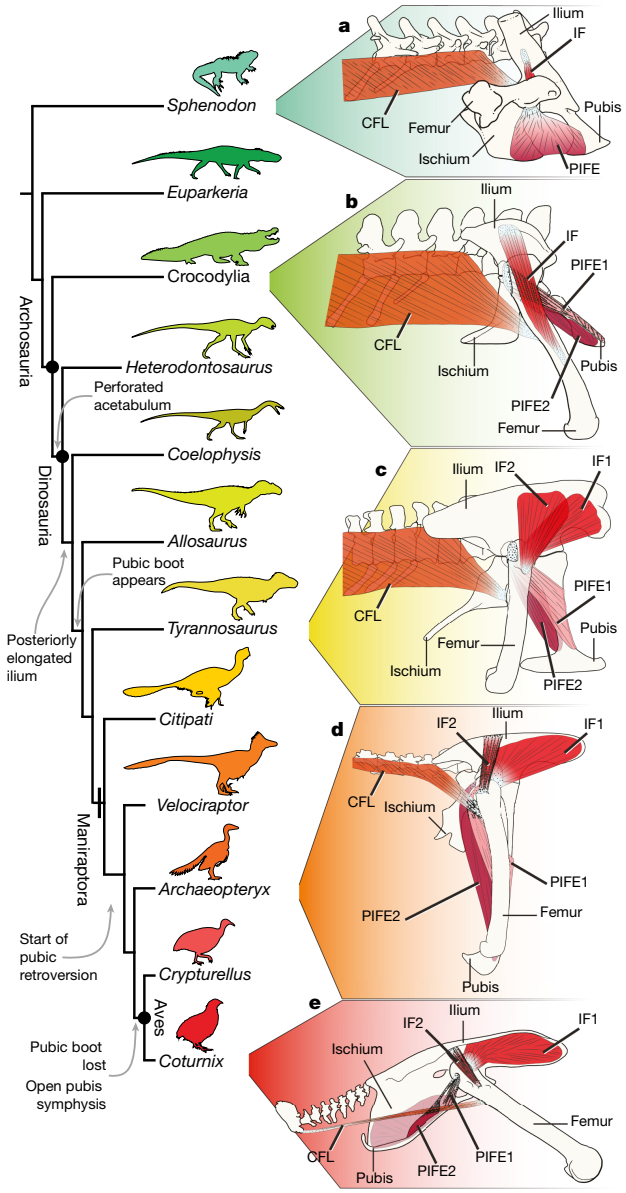

Fig. 1 | Archosaurian phylogeny and pelvic evolution on the line to birds. Through evolutionary time, the ilium extends both anteriorly and posteriorly, the pubis retroverts, the tail becomes proportionally reduced and the acetabulum becomes perforated. The IF (M. iliofemoralis and homologues) splits into two muscles (IF1, M. iliotrochantericus caudalis; IF2, M. iliofemoralis externus), the larger of which becomes directed anteriorly; the CFL (M. caudofemoralis longus and homologue) is reduced; and PIFE1+2 (Mm. puboischiofemoralis externus 1 et 2 and homologues) change their lines of action as the pubis retroverts. **a**, *Sphenodon* pelvis. **b**, *Alligator* pelvis. **c**, *Tyrannosaurus* pelvis. **d**, *Archaeopteryx* pelvis. **e**, *Coturnix* pelvis, with PIFE2 inserting on the medial face of the ischium. Note that the homology of the *Sphenodon* PIFE and the archosaurian PIFE1 is ambiguous.

Here we describe a striking instance of sequential terminal addition in the evolution of the avian pelvis: an ancestral reptilian configuration in the earliest developmental stages transitions step by step to the derived avian condition in an order that mirrors the morphological evolution of non-avian dinosaurs to living birds. We captured three-dimensional (3D) representations of crocodylian and avian embryonic musculoskeletal tissues at higher resolutions and earlier stages than has previously been possible by using a variation of the CLARITY[32] protocol to make a series of embryonic pelvic regions optically transparent while retaining fine-scale (that is, subcellular) structure. We then immunostained relevant embryonic tissues (cartilaginous primordia, cartilage, muscle and nerve) before creating *z* stacks of confocal microscopy images for processing with computed tomography (CT) software to form 3D models of the embryonic tissues (Methods).

Anatomy of the developing pelvis

As an extant archosaurian outgroup, we used the crocodilian *Alligator mississippiensis*. We found little overall shape change in the prehatching pelvic ontogeny of *Alligator* (Fig. 2, Extended Data Figs. 1 and 2, and Supplementary Information): embryonic *Alligator* pelves strongly resembled adult pelves throughout development, except that the pubes were separate from each other in early stages (Extended Data Fig. 5). We next examined the development of the avian skeletal pelvis using the Japanese quail *Coturnix coturnix japonica*. In the *Coturnix* embryo, the tail shifted from a long, typically 'reptilian' tail to a proportionally shortened nub (Fig. 3c). Early in avian pelvic morphogenesis, when the cartilaginous precursors of the pelvic elements were beginning to condense, the pubis faced anteriorly instead of posteriorly as in adult birds, a condition that persisted through several early stages (Fig. 3b). A transient pubic 'boot' or expanded distal end, as in basal tetanuran theropods, appeared and then disappeared during these stages (Figs. 1 and 3a,b). At later stages, the retroverted pubis, apomorphic for Paraves, gradually developed (Fig. 3a,b). Initially in development, the ilium was diminutive in the manner of early archosaurs. Subsequently, it became elongated posteriorly, the apomorphic condition for early Dinosauria (Fig. 1). Only at late developmental stages did it extend anteriorly to produce the derived avialan and then avian conditions (Fig. 3b). The hip socket remained imperforate throughout embryonic development[33] (Fig. 3b). Notably, the sequence of addition of derived characters in development mirrors their order of appearance in evolution (Figs. 3 and 4). This pattern was present in the pelvic ontogeny of another galloanseriform (chick, *Gallus gallus domesticus*), a paleognath (Chilean tinamou, *Nothoprocta perdicaria*) and (at least in part) a neoavian (budgerigar, *Melopsittacus undulatus*), indicating that the overall transformation is ancestral for Aves and may persist into later-diverging avian clades (Extended Data Fig. 6). Therefore, the avian pelvis evolved largely through the sequential addition of morphological innovations at the terminus of morphogenesis. The only exceptions to this rule were two derived avian states that resembled early ancestral/developmental morphologies (that is, instances of localized paedomorphosis): the broad, flat avian ischium resembled the early embryonic and ancestral archosaurian condition more than it did the intermediate dinosaurian conditions (Figs. 1 and 3a) and the pubic symphysis remained open throughout avian development, as it is in early embryonic pelves across tetrapods (Supplementary Information and Extended Data Fig. 5). Sequential addition of derived characters during avian pelvic development has remained largely undocumented, probably because many of these characters (such as the transient pubic boot) occur very early in pre-cartilage masses that are not easily visualized using traditional stains such as Alcian blue.

Myology and neuroanatomy of the developing hip

Because the skeletal, muscular and nervous systems are integrated functionally, developmentally and evolutionarily, we next characterized the comparative development of avian muscles and nerves with reference to proposed ancestral forms. Bone scars marking areas of muscle attachment on the pelvis and hindlimb have been used tentatively to reconstruct the musculature of non-avian dinosaurs[2,34], allowing ancestral states for soft tissues to be hypothesized (Fig. 1). The presence of ancestral states in the avian skeletal pelvis suggests that correspondence between embryonic and hypothesized ancestral muscular arrangements may be used reciprocally, both supporting these reconstructions and illuminating how ancestral states appear in avian development.

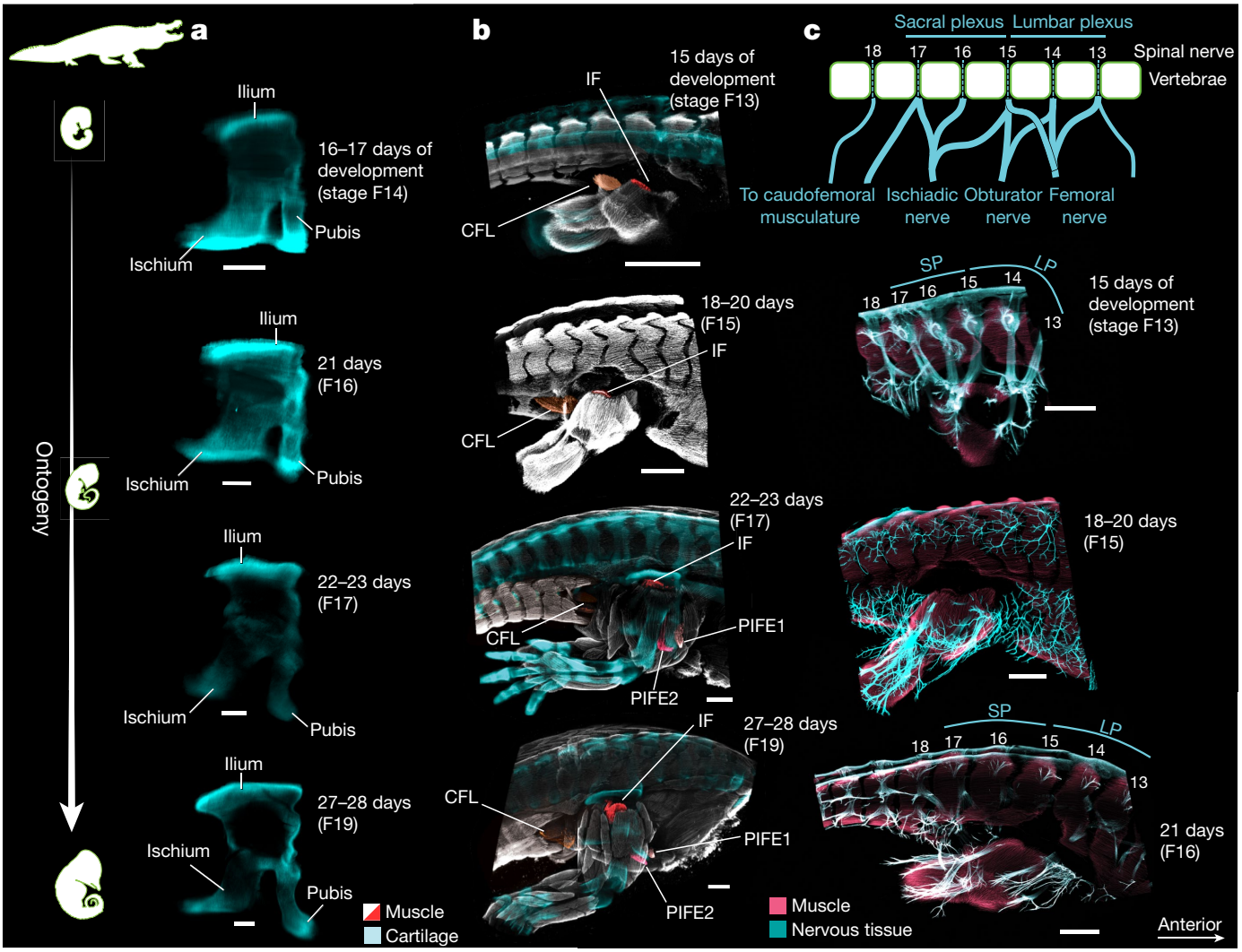

Fig. 2 | Embryological series of *A. mississippiensis* pelves showing that *Alligator* retains the same states throughout prehatching ontogeny. a, The ilium, ischium and pubis all retain similar states and morphologies throughout ontogeny. **b**, During ontogeny, the IF (M. iliofemoralis) begins similarly to in the avian condition but remains smaller and situated further back on the ilium; PIFE1+2 (Mm. puboischiofemoralis externus 1 et 2) are late to differentiate, similarly to in the avian condition, but retain the same line of action because the pubis does not retrovert. Muscles that are not highlighted are in grey. **c**, Pelvic spinal nerve arrangement in *Alligator* (top), probably retaining the ancestral archosaurian condition[35,48,49], and nerves in *Alligator* embryos (bottom). LP, lumbar plexus; SP, sacral plexus. Embryonic stages follow those in ref. [50]. Muscle tissue was stained for myosin heavy chain, nervous tissue was stained for neurofilament and cartilage was stained for collagen II. Scale bars: 1 mm in **a**, 2 mm in **b**,**c**.

The muscles substantially contributing to hindlimb-driven locomotion are thought to have shifted during the reduction of the tail along the avian stem: in the ancestral archosaurian state, retained in living crocodylians[24], M. caudofemoralis longus (CFL; Fig. 1) of the tail is the main rearward driver of the leg and M. iliofemoralis (IF; Fig. 1) acts as a limb abductor[1,21,23,24]. The IF expanded anteriorly along with the ilium, shifting from leg abduction to femoral long-axis rotation to facilitate the uniquely avian style of bipedalism[1,21,23]. The IF of the avian embryo remained relatively small and situated posteriorly on the ilium at earlier developmental stages (Fig. 3c), similarly to that of *Alligator* (Figs. 1 and 2b). It expanded anteriorly with the ilium as ontogeny proceeded. Although the ancestrally small IF split into two muscles early along the avian stem lineage[2] (IF1+2; Fig. 1), IF cleavage into two heads was not visible in our sampled developmental stages. Because a single-headed IF was present in all avian embryos sampled (Extended Data Fig. 6), with cleavage of other muscles clearly visible (for example, PIFE1+2), we interpret this as a real signal and not methodological imprecision. In sum, earlier embryonic stages resemble the small IF of the ancestral archosaur while later developmental stages resemble the condition typical of non-avian dinosaurs and birds in being expanded and anteriorly directed.

During avian evolution, two muscles that extend from the pubis to the femur, Mm. puboischiofemoralis externus 1 et 2 (PIFE1+2), completely shifted their lines of action as the pubis retroverted and they were carried posteriorly past the hip joint. During avian ontogeny, differentiation of PIFE1+2 from the main muscle mass was delayed relative to *Alligator*, occurring only after the pubis began retroversion during development. We interpret this delay as a functional consequence of retroversion, with a delay in differentiation necessary to enable retroversion and the consequent reversal in muscular line of action.

We found, somewhat unexpectedly, that nerve development appeared to be independent from musculoskeletal development: the derived condition of the avian nervous arrangement was present throughout ontogeny (Fig. 3d). The lumbosacral plexus of the developing embryo was similar to that of the adult *Coturnix* at even the beginning of nervous development and differentiation (that is, stage HH24, ~4 days of development) and different from that of the ancestral diapsid condition[35] typified by *Alligator* (Fig. 2c), despite the absence

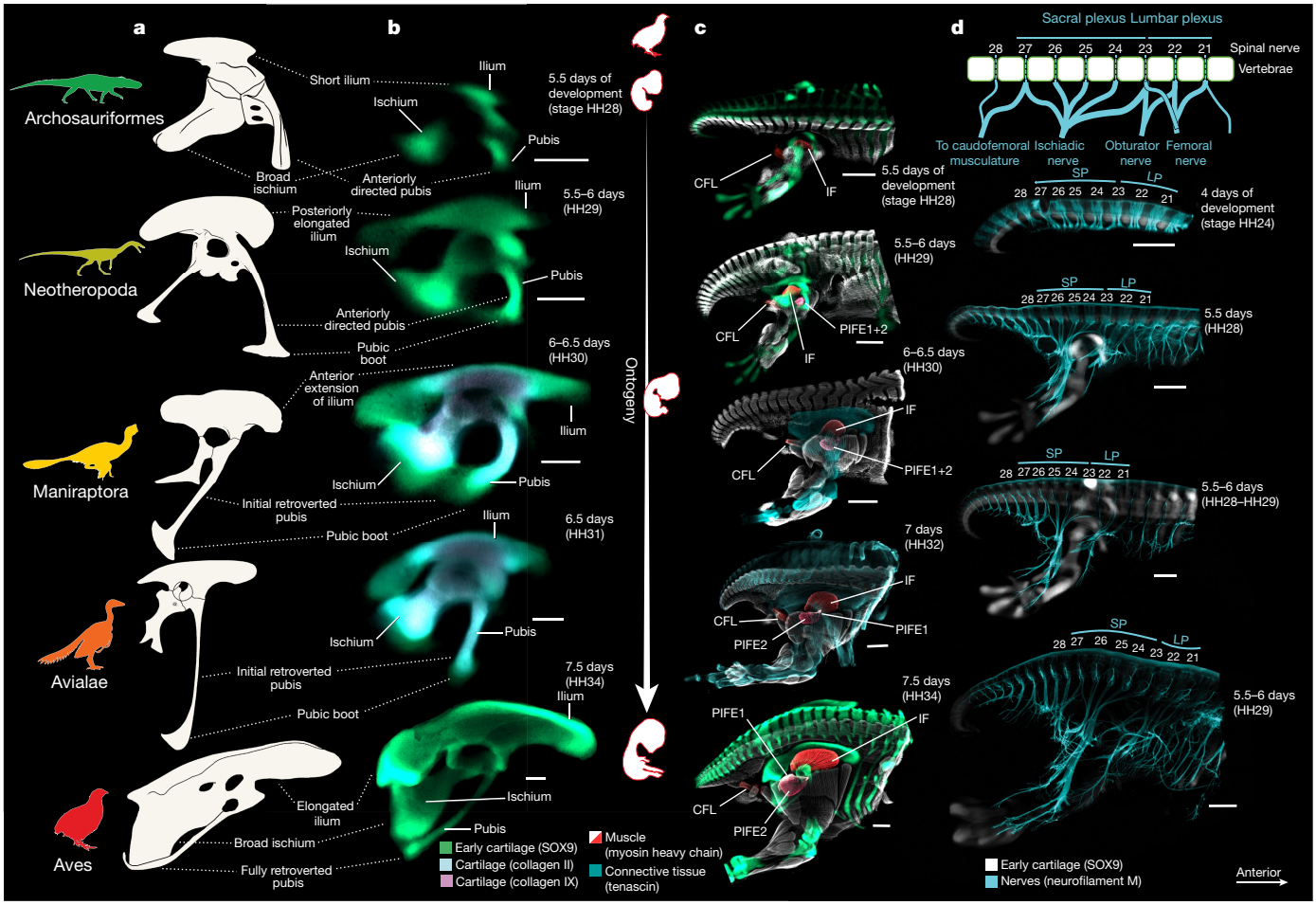

Fig. 3 | Embryological series of *C. coturnix japonica* (Japanese quail) showing the transition from ancestral to derived pelvic states across avian prehatching ontogeny. a, Pelvic reconstructions along the evolutionary transition to living birds. Note that pelves are shown as examples of character states and are not in one-to-one correspondence with ontogenetic stages. **b**, During ontogeny, the ilium extends first posteriorly and then anteriorly, the pubis retroverts, the tail becomes relatively reduced and a transient pubic boot appears at intermediate ontogenetic stages. **c**, The CFL (M. caudofemoralis longus homologue) is large during early ontogenetic stages; the IF (M. iliofemoralis homologue) originates smaller and further back on the ilium before expanding anteriorly to the derived condition and never splits into two muscles as seen in the adult; and PIFE1+2 (Mm. puboischiofemoralis externus 1 et 2 homologues) fail to fully differentiate until after the pubis is retroverted. Muscles that are not highlighted are in grey. **d**, The derived pelvic spinal nerve arrangement in Aves (top), with additional spinal nerves contributing to the sacral plexus[35,48,49] and nerves in *Coturnix* embryos (bottom). Embryonic stages follow those in ref. [51] as described for *Coturnix*[52]. Scale bars: 1 mm in **b**,**d**, 2 mm in **c**.

of the typical avian extended sacrum in early avian morphogenesis (Extended Data Figs. 3 and 4). This suggests that there are early constraints on nervous development[36–38] that are independent from those on the pelvic musculoskeletal system. Apparently, differing constraints can influence the ways in which ancestral and derived states appear in ontogeny among different anatomical regions and even among tissues of the same anatomical region.

Comparative shape analyses

To quantify and formally compare developmental and phylogenetic trajectories, we used a 3D geometric morphometrics approach (Fig. 4). We constructed 3D polygon meshes of hemipelves (the ilium, ischium and pubis of one anatomical side) representing embryonic skeletal precursors that were directly comparable to meshes constructed through 3D surface scanning and CT scanning of skeletal material. Thirteen landmarks allowed us to capture a comprehensive sample of variation across a sample of embryonic *Alligator* and avian pelves in combination with a new assemblage of non-embryonic reptilian pelves that focused on taxa along the avian stem, extant crocodylians, the archosauriform *Euparkeria capensis* and the lepidosaur *Sphenodon punctatus* (Supplementary Table 3). The first two principal components (PCs) described the majority of variation in the sample (Fig. 4a), with all others each describing <15%. Both evolutionary and ontogenetic signals in the sample were largely accounted for by PC1, being driven primarily by the anteroposterior elongation of the ilium and the retroversion of the pubis (Fig. 4b). Taxa with plesiomorphic reptilian/archosaurian pelves, including *Sphenodon*, the stem archosaur *Euparkeria* and living crocodylians, clustered together along with all *Alligator* embryos and early diverging non-avian theropods (for example, *Coelophysis* and *Allosaurus*; Fig. 4a and Extended Data Fig. 5). Birds and *Heterodontosaurus*, an early ornithischian dinosaur with a convergent pelvic morphology, were well separated from this group along PC1. The lineage of non-avian theropods and their reconstructed common ancestors bridged the gap between ancestral and derived pelvis morphologies across the morphospace. Quantification of the allometric trajectories of *Coturnix* and *Alligator* pelvic shape change identified heterochronic acceleration, not peramorphosis, on the part of *Coturnix* (Extended Data Fig. 9), supporting our interpretation of terminal addition in avian pelvic development. The *Coturnix* and *Alligator* trajectories were statistically divergent. In the linear model, centroid size alone was statistically significant but explained little of the variation in

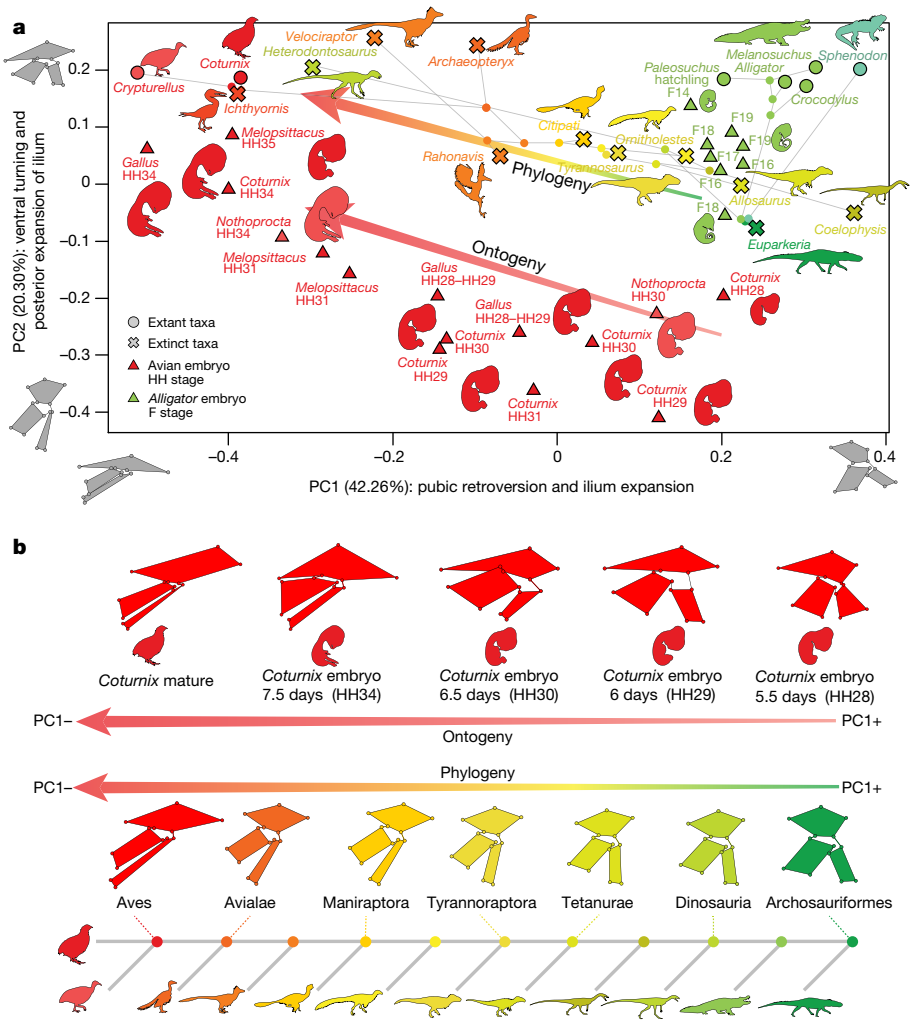

Fig. 4 | Avian morphogenesis extends across 3D geometric morphometric PC space from ancestral to derived conditions. a, PC1 and PC2 with ancestral states, phylogenetic relationships, and embryonic and osteological samples. **b**, Ontogenetic shape changes across PC1 are mirrored in reconstructed ancestral state changes across PC1. Avian embryonic stages follow those in refs. [51,52], while *A. mississippiensis* embryo stages follow those in ref. [50]. Phylogeny and colours follow Fig. 1.

shape ($R^2 = 0.08$, $F_{1,16} = 2.66$, $P = 0.035$). Both species alone ($R^2 = 0.40$, $F_{1,16} = 13.03$, $P < 0.001$) and the interaction between species and centroid size (that is, the different ontogenies; $R^2 = 0.19$, $F_{1,16} = 6.60$, $P < 0.001$) explained more variation.

The ontogenetic series of embryonic avian pelves followed a trajectory parallel to the evolutionary sequence across PC1, extending from the ancestral region of the morphospace to the derived region. Although the overall trajectories were parallel, the evolutionary sequence and the ontogenetic series of avian embryos diverged along the PC2 axis, distinguished primarily by the degree of ventral bowing and posterior expansion of the ilium (Fig. 4a). The embryonic avian series extended across novel morphospace on the negative region of PC2, whereas extant crocodylians and *Sphenodon* were differentiated from the ancestral archosaurian condition in the positive region of PC2; notably, the earliest *Coturnix* embryo (HH28) plotted closer than any non-embryonic crocodylian to the ancestral archosaurian condition. The *Alligator* embryonic series was offset from the mature crocodylians along PC2 and plotted more closely to *Euparkeria* because some of the *Alligator* embryos had ilia that were more plesiomorphically elongate than those of mature crocodylians. Most of the variation in our sample could be described in lateral view, and two-dimensional (2D) geometric morphometric analysis (which permits greater taxon inclusion) showed nearly identical relationships in morphospace (Extended Data Fig. 7a; Mantel test of Procrustes distances: $R = 0.96$, $P = 0.001$; Methods). Cluster analysis showed the expected dichotomy between ancestral and derived morphologies in the non-embryonic data, with the series of avian embryos split among clusters in the 2D analysis and forming their own cluster (excluding the most mature individuals) in the 3D analysis (Extended Data Fig. 7a,b). Therefore, avian ontogeny and phylogeny form parallel morphological trajectories: the avian pelvis possesses many plesiomorphic states in early organogenesis that change to derived states in roughly phylogenetic order, with the intermediate embryos diverging slightly in shape along PC2. Indeed, in the absence of middle-stage embryonic pelves, the ontogenetic and phylogenetic paths through morphospace were even more similar (Extended Data Fig. 7c).

Modularity and integration

Development influences the integration of phenotypic traits into modules (covariant traits that are weakly correlated with other traits[39–41]), which have had important roles in archosaurian and avian phenotypic evolution[42,43]. We therefore investigated phenotypic covariance in the archosaurian pelvis. Covariance among traits can promote the evolution of extreme morphologies along an evolutionary axis of least resistance[44], so these processes are especially

important to the evolution of highly divergent anatomical regions such as the avian pelvis[45]. We first tested for the presence of covariant portions of the archosaurian pelvis by splitting landmarks into a priori anatomical subsets for the ilium, ischium and pubis and conducting geometric morphometrics on these subsets. We found that most subsets contained a nearly identical signal to the overall pelvic analysis, with the only major divergences from this pattern in the ischium and ischium + pubis subsets (Extended Data Fig. 8). This is potentially because the plate-like embryonic *Alligator* and *Coturnix* ischia are more similar to each other than they are to the rod-like ischia of non-avian theropods (for example, see Fig. 1). We also quantified covariance by examining statistical differences between the covariance ratios (CRs)[46] of a priori subsets and the CR values of randomly distributed subsets of landmarks. Only the anteroposterior extremities of the ilium and the distal extremity of the pubis (that is, the traits described by PC1; Fig. 4a) were phenotypically covariant (CR = 0.94, $P = 0.0478$; Extended Data Fig. 8g), and all other anatomical subsets failed to meet the threshold for statistical significance ($P = 0.152–0.489$). This set of traits remained significant both for non-paravian archosaurs (CR = 0.889, $P = 0.013$) and for only those taxa with retroverted pubes (CR = 0.900, $P = 0.006$) as well as an independent dataset[47] of 149 extant avian pelves (CR = 0.812, $P = 0.036$).

We further explored pelvic covariance by taking relevant measurements (for example, the anterior extension of the ilium and length of the pubis) normalized to acetabulum width, as well as the degree of pubic retroversion, and constructing a variance–covariance matrix of these factors (Methods). Unexpectedly, given the seemingly extreme differences between the ancestral archosaurian/dinosaurian and derived avian pelvic conditions[45] (Fig. 4), the covariances among different pelvic proportions were nearly identical between paravians (with retroverted pubes) and non-paravian archosaurs (with anteriorly directed pubes) (Extended Data Fig. 10). For example, in both groups, the anterior length of the ilium increased as the pubic angle shifted posteriorly; even in groups without pubic retroversion, this relationship held. This indicates that birds do not have pelvic covariances fundamentally different from those of their non-avian relatives, but that the avian pelvis is an extreme case of covariation conserved across non-avian theropods and other archosaurs. Therefore, unexpectedly, despite the extreme divergence of the avian pelvis relative to other archosaurs, distinctive transformations such as the anteroposterior extension and the lengthening and retroversion of the pubis occur together within a consistent covariant relationship among archosaurs.

Origin of the bird hip by terminal addition

We suggest that phenotypic covariance in evolution and development, and terminal addition in the musculoskeletal (but not the nervous) architecture of the archosaurian pelvis, was key to the origin of the highly derived pelvic morphology of Aves, promoting evolution of the disparate morphology required for the unique avian form of hindlimb locomotion[1,10,21–24]. This covariance of structure also suggests the tantalizing possibility of a mechanism—phenotypic modularity—promoting the tendency of ancestral states to persist in the development of vertebrates (terminal addition)[8,9]. We propose that a mechanism compelling persistent covariation of proportions across the archosaurian pelvis underlies terminal addition in evolution of the extreme morphology present in birds. Continuous covariation across the pelvis in the evolution of the avian lineage could produce morphological changes primarily to the axis of least resistance[44] determined by this covariation: changes would occur by truncation of development or, as seen along the avian line, by extension, manifesting as terminal addition. This not only suggests an explanation for the retention of ancestral states in development, especially in later developmental stages, but also provides specific criteria for detecting other cases of terminal addition. Such cases may be common across major evolutionary transitions.

Online content

Any methods, additional references, Nature Research reporting summaries, source data, extended data, supplementary information, acknowledgements, peer review information; details of author contributions and competing interests; and statements of data and code availability are available at https://doi.org/10.1038/s41586-022-04982-w.

1. Gatesy, S. M. in *Functional Morphology in Vertebrate Paleontology* (ed. Thomason, J. J.) 219–234 (Cambridge University Press, 1995).
2. Hutchinson, J. R. The evolution of pelvic osteology and soft tissues on the line to extant birds (Neornithes). *Zool. J. Linnean Soc.* **131**, 123–168 (2001).
3. Turner, A. H., Makovicky, P. J. & Norell, M. A. A review of dromaeosaurid systematics and paravian phylogeny. *Bull. Am. Museum Nat. Hist.* **371**, 1–206 (2012).
4. Ostrom, J. H. On a new specimen of the Lower Cretaceous theropod dinosaur *Deinonychus antirrhopus*. *Breviora* **439**, 1–21 (1976).
5. Bunge, A. *Untersuchungen zur Entwickelungsgeschichte des Beckengürtels der Amphibien, Reptilien, und Vögel*. PhD thesis, Universität Dorpat (1880).
6. Johnson, A. On the development of the pelvic girdle and skeleton of the hind limb of the chick. *Q. J. Microsc. Sci.* **23**, 399–411 (1883).
7. Mehnert, E. Untersuchungen über die entwisklung des os pelvis der vögel. *Morphologisches Jahrbuch* **13**, 259–295 (1887).
8. Gould, S. J. *Ontogeny and Phylogeny* (Harvard University Press, 1977).
9. Mayr, E. Recapitulation reinterpreted: the somatic program. *Q. Rev. Biol.* **69**, 223–232 (1994).
10. Abzhanov, A. von Baer's law for the ages: lost and found principles of developmental evolution. *Trends Genet.* **29**, 712–722 (2013).
11. Diogo, R., Smith, C. M. & Ziermann, J. M. Evolutionary developmental pathology and anthropology: a new field linking development, comparative anatomy, human evolution, morphological variations and defects, and medicine. *Dev. Dyn.* **244**, 1357–1374 (2015).
12. Ksepka, D. T. Feathered dinosaurs. *Curr. Biol.* **30**, R1347–R1353 (2020).
13. Lowe, C. B., Clarke, J. A., Baker, A. J., Haussler, D. & Edwards, S. V. Feather development genes and associated regulatory innovation predate the origin of Dinosauria. *Mol. Biol. Evol.* **32**, 23–28 (2015).
14. Bhullar, B.-A. S. et al. How to make a bird skull: major transitions in the evolution of the avian cranium, paedomorphosis, and the beak as a surrogate hand. *Integr. Comp. Biol.* **56**, 389–403 (2016).
15. Fabbri, M. et al. The skull roof tracks the brain during the evolution and development of reptiles including birds. *Nat. Ecol. Evol.* **1**, 1543–1550 (2017).
16. Bhullar, B.-A. S. et al. A molecular mechanism for the origin of a key evolutionary innovation, the bird beak and palate, revealed by an integrative approach to major transitions in vertebrate history. *Evolution* **69**, 1665–1677 (2015).
17. Louchart, A. & Viriot, L. From snout to beak: the loss of teeth in birds. *Trends Ecol. Evol.* **26**, 663–673 (2011).
18. O'Connor, P. M. Evolution of archosaurian body plans: skeletal adaptations of an air-sac-based breathing apparatus in birds and other archosaurs. *J. Exp. Zool. A* **311A**, 629–646 (2009).
19. Heers, A. M. & Dial, K. P. From extant to extinct: locomotor ontogeny and the evolution of avian flight. *Trends Ecol. Evol.* **27**, 296–305 (2012).
20. Mayr, G. Evolution of avian breeding strategies and its relation to the habitat preferences of Mesozoic birds. *Evol. Ecol.* **31**, 131–141 (2017).
21. Gatesy, S. M. Caudofemoral musculature and the evolution of theropod locomotion. *Paleobiology* **16**, 170–186 (1990).
22. Gatesy, S. M. & Dial, K. P. Locomotor modules and the evolution of avian flight. *Evolution* **50**, 331–340 (1996).
23. Hutchinson, J. R. The evolution of locomotion in archosaurs. *C. R. Palevol.* **5**, 519–530 (2006).
24. Hutchinson, J. R. & Gatesy, S. M. Adductors, abductors, and the evolution of archosaur locomotion. *Paleobiology* **26**, 734–751 (2000).
25. Organ, C. L., Shedlock, A. M., Meade, A., Pagel, M. & Edwards, S. V. Origin of avian genome size and structure in non-avian dinosaurs. *Nature* **446**, 180–184 (2007).
26. Gegenbaur, C. *Gundriss der Vergleichenden Anatomie* (Engelmann, 1878).
27. Huxley, T. H. Further evidence of the affinity between the dinosaurian reptiles and birds. *Q. J. Geol. Soc. Lond.* **26**, 12–31 (1870).
28. Carroll, S. B. Evo-devo and an expanding evolutionary synthesis: a genetic theory of morphological evolution. *Cell* **134**, 25–36 (2008).
29. Romer, A. S. The development of the thigh musculature of the chick. *J. Morphol. Physiol.* **43**, 347–385 (1927).
30. Schroeter, S. & Tosney, K. W. Spatial and temporal patterns of muscle cleavage in the chick thigh and their value as criteria for homology. *Am. J. Anat.* **191**, 325–350 (1991).
31. Kardong, K. V. *Vertebrates: Comparative Anatomy, Function, Evolution* 8th edn (McGraw-Hill Education, 2019).
32. Chung, K. et al. Structural and molecular interrogation of intact biological systems. *Nature* **497**, 332–337 (2013).
33. Egawa, S., Saito, D., Abe, G. & Tamura, K. Morphogenetic mechanism of the acquisition of the dinosaur-type acetabulum. *R. Soc. Open Sci.* **5**, 180604 (2018).
34. Hutchinson, J. R. The evolution of hindlimb tendons and muscles on the line to crown-group birds. *Comp. Biochem. Physiol. A* **133**, 1051–1086 (2002).
35. Giffin, E. B. Postcranial paleoneurology of the Diapsida. *J. Zool.* **235**, 389–410 (1995).
36. Carpenter, E. M. *Hox* genes and spinal cord development. *Dev. Neurosci.* **24**, 24–34 (2002).
37. Gaunt, S. J. Evolutionary shifts of vertebrate structures and *Hox* expression up and down the axial series of segments: a consideration of possible mechanisms. *Int. J. Dev. Biol.* **44**, 109–117 (2000).

38. Diogo, R., Ziermann, J., Molnar, J., Siomava, N. & Abdala, V. *Muscles of Chordates: Development, Homologies and Evolution* (Taylor & Francis, 2018).
39. Felice, R. N., Randau, M. & Goswami, A. A fly in a tube: macroevolutionary expectations for integrated phenotypes. *Evolution* **72**, 2580–2594 (2018).
40. Olson, E. C. & Miller, R. L. *Morphological Integration* (University of Chicago Press, 1958).
41. Schlosser, G. in *Modularity in Development and Evolution* (eds Schlosser, G. & Wagner, G. P.) 519–582 (University of Chicago Press, 2004).
42. Lee, H. W., Esteve-Altava, B. & Abzhanov, A. Evolutionary and ontogenetic changes of the anatomical organization and modularity in the skull of archosaurs. *Sci. Rep.* **10**, 16138 (2020).
43. Felice, R. N. et al. Evolutionary integration and modularity in the archosaur cranium. *Integr. Comp. Biol.* **59**, 371–382 (2019).
44. Goswami, A., Smaers, J. B., Soligo, C. & Polly, P. D. The macroevolutionary consequences of phenotypic integration: from development to deep time. *Philos. Trans. R. Soc. B* **369**, 20130254 (2014).
45. Iijima, M. & Kobayashi, Y. Convergences and trends in the evolution of the archosaur pelvis. *Paleobiology* **40**, 608–624 (2014).
46. Adams, D. C. Evaluating modularity in morphometric data: challenges with the RV coefficient and a new test measure. *Methods Ecol. Evol.* **7**, 565–572 (2016).
47. Bjarnason, A. & Benson, R. A 3D geometric morphometric dataset quantifying skeletal variation in birds. *MorphoMuseuM* **7**, e125 (2021).
48. Giffin, E. B. Endosacral enlrgements in dinosaurs. *Mod. Geol.* **16**, 101–112 (1991).
49. Giffin, E. B. Paleoneurology: reconstructing the nervous systems of dinosaurs. *Paleontol. Soc. Special Pub.* **7**, 229–242 (1994).
50. Ferguson, M. W. J. in *Biology of the Reptilia* Vol. 14 (eds Gans, C. et al.) 329–492 (John Wiley and Sons, 1985).

Methods

Clearing embryonic pelves with the CLARITY[32] protocol

We incubated Japanese quail (*C. coturnix japonica*) eggs for between 4–7.5 days, removing embryos and fixing in 4% paraformaldehyde (PFA) at HH stages 24–34 in plastic test tubes for 3 days (see refs. [51,52]) before dehydrating them with 100% methanol (four 15-min washes in 100% PBS followed by four 15-min washes in 100% methanol). This same procedure was conducted on domestic chicken (*G. gallus domesticus*) embryos at stages HH29 and HH34, Chilean tinamou (*N. perdicaria*) embryos at stages HH30 and HH34, and budgerigar (*M. undulatus*) embryos at stages HH31 and HH35. We selected *A. mississippiensis* embryos from between stages F13–F20 (15–30 days of incubation; stages following ref. [50]). *Coturnix* eggs and embryos were sourced from Stromberg's Chickens; *Gallus* eggs and embryos were from the University of Connecticut Poultry Farm and Poultry Resource Unit; *Melopsittacus* and *Nothoprocta* embryos were from the Laboratory of Ontogeny and Phylogeny, Universidad de Chile (A. Vargas, principal investigator); and *A. mississippiensis* eggs were collected from the Rockefeller Wildlife Refuge. Embryos were removed and fixed in PFA before being dehydrated into 100% methanol and stored at −20 °C.

To bleach the embryos, we replaced the methanol solution with a mixture of methanol, peroxide and DMSO and placed them under a UV lamp with motion for 24 h. After a series of washes to progressively replace the methanol with 100% PBS, we removed the 1× PBS solution and replaced it with 200 ml of modified CLARITY solution to create a hydrogel monomer (160 ml of water, 20 ml of 10× PBS, 20 ml of acrylamide (40%), 0.5 g of V-040 as an initiator and 250 µl of bis-acrylamide) before placing these samples in a 4 °C refrigerator under motion for 24 h. Bis-acrylamide in particular is an addition to cross-link samples, allowing for greater tissue integrity when the embryo is later dissected. Following this step, we placed rubber stoppers containing two syringe needles connected to valves on the test tubes. One stopper of each needle was connected to nitrogen gas, and one was connected to a vacuum; air was progressively replaced with nitrogen by running alternating rounds of vacuum and nitrogen gas into the stopper. After closing the valves, we placed the test tubes in a 37 °C water bath under motion for 3 h, keeping the stopper on at all times to prevent oxygen from entering. Following this, the CLARITY solution was replaced with a PBS detergent solution (PBST; 0.1 M PBS, 0.5% Triton X-100) before placing samples under motion and light for 1 h. Following another round of washing with PBST and motion for 1 h, we replaced the PBST with HCl (1 M HCl diluted 5:2 with deionized water) and placed the samples in a 37 °C heater under motion for 1 h, before washing twice with PBST again. We then dissected embryos with small scissors transversely at the torso to preserve the pelvis, hindlimb and tail morphology while keeping the sample as small as possible for confocal microscopy. We then placed the embryonic hips in 4% SDS, an ionic detergent, and placed them at 37 °C under motion for roughly 1 week or until the hips were clear. See the Supplementary Information for a more detailed description of the modified CLARITY protocol.

Immunostaining of embryonic pelves

We immunostained the cleared embryonic hips for proteins expressed in developing cartilage, connective tissue, skeletal muscles and nerves to capture the morphology of pelvic development at the selected stages. We accomplished this using indirect immunofluorescence, with primary antibodies directed against target antigens (proteins), which were in turn antigens of secondary antibodies conjugated to a dye that fluoresced when exposed to a specific wavelength of light. Although Alcian blue staining of embryonic cartilage is widely used[53–57], including in the staining of avian pelves[58–62], because this staining works through binding to chemicals within the cartilaginous extracellular matrix[55,57] it is most appropriate for staining mature cartilage at later developmental stages[54]. Therefore, recent studies of avian pelvic ontogeny that used Alcian blue staining were focused on visualizing mature cartilage and ossification sequences (stages HH33 and later) and not on the stages of ontogeny characterized by precartilage mesenchymal condensation or early-stage cartilage with immature chondrocytes. Because we were interested in investigating these earlier stages of cartilage differentiation/formation and early skeletal morphogenesis, we used mouse and rabbit primary antibodies to stain for SOX9 (a transcription factor expressed early in chondrocyte differentiation[63–65]), collagen type II (expressed during early cartilage formation[66–69]) and collagen type IX (expressed during endochondral cartilage maturation[66,67,69,70]). We also stained for myosin heavy chain (MF-20), expressed in skeletal muscles[71,72], and neurofilament M (NF-M), expressed in nerve tissue[73]. We further stained for more general connective tissues with collagen I and tenascin, but these were not as successful as the other stains and we do not discuss them here. We were unable to immunostain for every protein of interest in every embryo because of antibody specificity constraints (for example, we could not stain two proteins of the same embryo with rabbit antibodies and expect to differentiate the tissues later because the secondary antibody would bind indiscriminately to all rabbit antibodies). Instead, we stained in combinations of 2–3 target proteins. Each of these combinations was used across a growth series of embryos. For *Coturnix*, we used three different combinations of proteins: SOX9, MF-20 and NF-M; MF-20, collagen I and tenascin; and SOX9, collagen II and collagen IX. We also used three different combinations of proteins for *Alligator*: SOX9 and collagen II; MF-20, NF-M and collagen I; and MF-20, collagen II and collagen I. For *Nothoprocta* and *Melopsittacus*, we stained for SOX9, MF-20 and NF-M, and for *Gallus* we stained for SOX9, MF-20 and collagen I. Note that SOX9-positive cells are present in both cartilage precursor cells and chondrocytes (that is, collagen II-positive cells; Extended Data Figs. 1a and 3b). See the Supplementary Information for details of our immunostaining protocol.

Confocal microscopy

To prepare the cleared and immunostained embryonic pelves for confocal microscopy, we first equilibrated them with refractive index matching solution (RIMS) and then placed the embryo on a small microscope dish and covered it with 20 ml of a 1% agarose RIMS solution. RIMS is necessary to prevent any optical distortion during confocal microscopy, and the 1% agarose gel allows the embryonic structure to be retained. The mounted embryo was then covered with a coverslip to prevent desiccation during microscopy. The details of making RIMS and the 1% agarose RIMS solution are available in the Supplementary Information.

We imaged the cleared and immunostained embryonic pelves with a Zeiss LSM 880 confocal microscope and associated Zen software, except for those of *Nothoprocta* and stage HH34 of *Gallus*, which were imaged with a Nikon TiE inverted spinning disc confocal microscope. We created tagged image file format (TIFF) stacks of images using the microscope by tiling the images captured by the confocal microscope to create whole-embryo 'slices', which were then assembled into a *z* stack of images. Embryo images were captured using a ×10 objective. The overall size of the scan area depended on the size of the embryo (*x*, *y* and *z* axes), and we used an overlap of 10% for fewer tiling artefacts. We used a 512 × 512 frame size, with a bidirectional scan with a speed of 8 and average of 4 to reduce noise, and we left the digital gain at 1. Each channel wavelength (that is, each laser used to excite florescence) was selected on the basis of the secondary antibodies used to stain the embryo being scanned (for example, if a secondary antibody that fluoresced at 488 nm was being imaged, one of the channels would be a 488-nm laser), with laser power set to 3.5 to prevent bleaching. The pinhole size was set by selecting '1 AU' to optimize and then clicking the down arrow once. Optimal gain was generally set between 600–800 but was sometimes lower if needed to properly visualize the embryonic tissues. We exported the confocal image stacks as Zeiss CZI (*.czi) files.

To prepare the image stacks to be imported into VGStudio MAX 3.3 (see below), we opened each *.czi file in Fiji[74] in ImageJ[75] (v.2.0.0),

ensured the colour mode for all channels was set as 'greyscale' (in the Channels Tool under the Colors menu) and then used the Split Channel command to split each channel into different windows. We saved each window as a different image sequence, which created a different TIFF stack for each channel to be imported into VGStudio individually, allowing the immunostained tissues to be visualized and segmented independently of each other.

CT scanning and construction of 3D meshes

We generated most of the 3D meshes used in these analyses through X-ray computed microtomographic (μCT) scanning of specimens or high-resolution research casts at Yale University. We used a Nikon XT H 225 ST scanner (85 kV, 90 μA) with 1-s exposure, 3,141 views and no frame averaging. Scans were segmented, and 3D meshes (stereolithography *.stl files) were created in Mimics (v.20). These 3D meshes were arranged and cleaned using Meshlab (v.2020.02). Additionally, the mesh of the mature *Alligator* pelvis was downloaded from Morphosource (project M22299), and the other extant, non-embryonic crocodylian pelves were downloaded from CrocBase (www.osf.io/6zamj). The *Coelophysis bauri* pelvis was scanned at The University of Texas at Austin, and we 3D surface scanned the pelves of *Allosaurus* and *Heterodontosaurus* at Yale University and Virginia Tech, respectively.

We visualized and segmented embryonic pelves from the confocal image stacks using VGStudio MAX 3.3. To form meshes from these segmented embryonic pelves, we first used the 'Surface determination' function in VGStudio MAX. Three to four different surfaces were determined for each pelvis: the first at the lowest grey value threshold that showed the surface of the pelvis and the last at the highest grey value threshold that continued to show surface features of the pelvis, with one or, in some cases, two intermediate thresholds to fully capture the overall morphology of the pelves. We constructed 3D triangle meshes from these surface determinations with the 'Convert to mesh' function in VGStudio MAX, using precise ray-based conversion with simplification. These meshes were then exported as stereolithography (*.stl) files for use in other applications. We then combined the different surfaces of each pelvis into one overall mesh that best captured the morphology of the embryonic pelvis in Meshlab, selecting extraneous faces and erasing them using the 'libfilter_select.dlb' command. We converted *.stl files to polygon file format (*.ply) files in Meshlab for geometric morphometric landmarking (see below). We used the stain for SOX9 to construct 3D meshes. See the Supplementary Information for details of specimens scanned and sources for meshes.

Geometric morphometrics

We selected 13 pelvic landmarks (types I and II)[76] on the basis of their ability to be consistently identified in all sampled taxa and in embryonic pelves of *Alligator* and *Coturnix* and how well they delineated the overall shape of the hemipelvis. We used hemipelves instead of pelves to reduce error caused by physical distortion of the embryo. Each cartilaginous hemipelvis remained intact and relatively undistorted, but especially in cases where the hemipelves were unfused (that is, in all avian stages and early *Alligator* stages) some hemipelves were shifted relative to the other during mounting as the embryo was laid on its side. Descriptions and illustrations of these landmarks are available in the Supplementary Information. We placed these landmarks on the 3D meshes using Landmark software (v.3.0.0.6), creating an NTSsys (*.nts) file of the resulting coordinates. For meshes that were too large to be loaded into Landmark, we reduced the number of faces to 1,000,000 using the 'quadratic edge clustering decimation' command in Meshlab, which simplified the meshes while retaining the overall shape and fine detail. Where necessary, we mirrored pelves so that they were uniformly oriented as anterior to the right. We conducted all geometric morphometric analyses and reconstructed ancestral geometric states using the R[77] package geomorph[78] (v.3.2.1). We estimated missing landmarks using the thin plate spline (TPS) method standard to geomorph and performed a generalized Procrustes analysis of the landmarks before performing a principal-coordinates analysis (PCA) of the resulting data. We used tpsDig[79] to assign the same 13 landmarks as 2D landmarks to lateral-view images of pelves captured in Meshlab (v.2020.02; for non-embryonic pelves) or VGStudio MAX 3.3 (for embryonic pelves), creating a TPS (*.tps) file. Subsets of these landmarks based on skeletal elements that were relevant to the evolutionary scenario (for example, an ilium subset and ilium + pubis subset) were partitioned in R for subsequent PCAs (Extended Data Figs. 6c and 7). We performed cluster analyses (Extended Data Fig. 7) using the R package NbClust[80], which determines the best-supported clusters under 34 different metrics. We used the *k*-means clustering method and performed these analyses on all PCs that explained >1% of the variance in the data.

Two taxa along the avian stem (*Shuvuuia* and *Balaur*) were present in our 2D geometric morphometric dataset but were not available for 3D analysis. The results of the 2D analysis appeared congruent with those of the 3D analysis (meaning that the absence of these taxa does not influence the interpretation of the 3D results), but to statistically test this congruence we followed the method described in ref. [81]. We constructed square matrices of pairwise Procrustes distances for each dataset in R, using the custom command 'proc.dist.matrix' created in ref. [81]. We then tested the similarity of these matrices with a Mantel test, using the command 'mantel' in the R package vegan[82], with the Pearson correlation method.

To quantify and visualize the allometric trajectories of *Coturnix* and *Alligator* in a geometric morphometrics context[83,84], we first used the 'procD.lm' command in geomorph to construct a multivariate linear model predicting Procrustes shape variables as a function of centroid size and species (shape ≈ size × species), testing the significance with 10,000 iterations. We used the 'anova.lm.rrpp' command to test model fit against a null model that did not account for differences between species (that is, a model that assumed that both taxa had the same ontogenetic trajectory), and this null model performed significantly worse ($P < 0.001$). Centroid size was used as a proxy for overall size; however, because not all 3D meshes were of the same scale and the exact scale for several meshes was not available, we instead used relative, unitless centroid sizes scaled to the smallest *Coturnix* embryo (stage HH28). This centroid size was assigned a value of 1, and all other *Coturnix* and *Alligator* specimens were assigned values to scale with this; for example, the mature *Coturnix* pelvis is 13.2 times larger than the pelvis at HH28, so its centroid size was given as 13.2. This is justified because the centroid size is the square root of the sum of the squared distances of all landmarks from their centroid[85], so centroid size scales linearly as size increases. We used the command 'plotAllometry' to visualize the allometric trajectories, plotting log-transformed centroid size against individual regression scores obtained from the linear model, which is a proxy for shape[83,86].

Modularity and variance–covariance calculations

We first explored evolutionary modularity in the pelvic landmarks by partitioning these landmarks a priori on the basis of anatomical regions and PC loadings and running the same PCA on this subset as with the overall dataset (Extended Data Fig. 8). We then tested for statistically significant evolutionary modules across the landmarks of our dataset using the 'modularity.test' function in the R package geomorph (v.3.2.1), testing various partitions of landmarks across the pelvis for statistically significant modules. To explore evidence for the same module in a larger sample of extant birds, we used 3D geometric morphometric landmark data from the synsacra of 149 extant birds, representing most major avian groups, compiled independently in ref. [47]. This consisted of 13 landmarks (semilandmarks were not used to be more directly comparable to our analyses), and the 'modularity.test' function was used as described above to test for a phenotypic module between the pubis and iliac extremities (landmarks 1–3, 5 and 6).

Finally, we used Fiji in ImageJ (v.2.0.0) to take proportional measurements of the pelves in our dataset (Extended Data Fig. 10) using images of the pelves in lateral view in Meshlab (v.2020.02). Measurements were normalized to the proximodistal width of the acetabulum between the pubic and iliac peduncles, which made normalization in taxa with and without perforated acetabula consistent. We partitioned the data into paravian, non-paravian (+ non-ornithischian) dinosaur and ornithischian datasets, constructed variance–covariance matrices for each of these partitions using the command 'cov' in bas+e R and plotted the 95% confidence ellipses of the data using the 'covEllipse' command in the R package heplots[87]. All data files used for analyses and all code are hosted on Dryad (https://doi.org/10.5061/dryad.xd2547dj2).

Further sources for phylogenetic relationships, pelvic reconstructions and silhouettes

Phylogenetic relationships follow the consensus of recent studies[3,88–96]. We reconstructed *Sphenodon* musculature following refs. [97–103], *Alligator* musculature following refs. [2,104–106], *Tyrannosaurus* musculature following ref. [104], *Archaeopteryx* musculature following refs. [2,21,34] and avian musculature following refs. [2,104,107,108]. In Figs. 1 and 3a, we drew the *Sphenodon* pelvis using ref. [99] as a primary reference, the *Alligator* pelvis using ref. [104], the *Tyrannosaurus* pelvis using ref. [104], the *Archaeopteryx* pelvis using refs. [109–111], the avian pelvis using ref. [104], the *Euparkeria* pelvis ('Archosauriformes', Fig. 3a) using ref. [112] and the *Ceratosaurus* pelvis ('Neotheropoda', Fig. 3a) using ref. [113]. The maniraptoran pelvis (Fig. 3a) is based on that in ref. [114] and the less autapomorphic pubis in ref. [115]. We identified embryonic avian muscles following refs. [29,30,116]. Silhouettes in Figs. 1–4 are licensed under Creative Commons Attribution 3.0 Unported (*Tyrannosaurus*, *Citipati*, *Balaur* and *Velociraptor*, E. Willoughby; *Heterodontosaurus* and *Coelophysis*, S. Hartman; *Crypturellus*, D. Naish) and Public Domain Dedication 1.0 (*Sphenodon*, S. Traver; *Euparkeria*, S. Hartman; *Rahonavis*, T.M. Keesey; *Archaeopteryx*, D. Pigdon; *Shuvuuia*, FunkMonk and *Ichthyornis*, E. Parker; *Allosaurus*, T. Dixon). All silhouettes are from Phylopic.org except for the *Alligator*, *Ornitholestes*, *Coturnix*, *Nothoprocta* and *Melopsittacus* silhouettes and all embryo silhouettes, which were created by C.T.G.

Reporting summary

Further information on research design is available in the Nature Research Reporting Summary linked to this paper.

Data availability

All data files used for analyses are hosted on Dryad (https://doi.org/10.5061/dryad.xd2547dj2). All fossils are reposited in recognized natural history institutions.

Code availability

All code is hosted on Dryad (https://doi.org/10.5061/dryad.xd2547dj2).

51. Hamburger, V. & Hamilton, H. L. A series of normal stages in the development of the chick embryo. *J. Morphol.* **88**, 49–92 (1951).
52. Ainsworth, S. J., Stanley, R. L. & Evans, D. J. R. Developmental stages of the Japanese quail. *J. Anat.* **216**, 3–15 (2010).
53. Dingerkus, G. & Uhler, D. Enzyme clearing of Alcian blue stained whole small vertebrates for demonstration of cartilage. *Stain Technol.* **52**, 229–232 (1977).
54. Ovchinnikov, D. Alcian blue/Alizarin red staining of cartilage and bone in mouse. *Cold Spring Harbor Protoc.* **2009**, pdb.prot5170 (2009).
55. Rigueur, D. & Lyons, K. M. Whole-mount skeletal staining. *Methods Mol. Biol.* **1130**, 113–121 (2014).
56. Schultze, O. Ueber herstellung und conservirung durchsichtiger embryonen zum stadium der skeletbildung. *Anatomischer Anzeiger* **13**, 3–5 (1897).
57. Horobin, R. W. in *Educational Guide Special Stains and H&E* 2nd edn (eds Kumar, G. L. & Kiernan, J. A.) 159–166 (Carpinteria, 2010).
58. Carril, J., Tambussi, C. P. & Rasskin-Gutman, D. The network ontogeny of the parrot: altriciality, dynamic skeletal assemblages, and the avian body plan. *Evol. Biol.* **48**, 41–53 (2021).
59. Maxwell, E. E. Comparative embryonic development of the skeleton of the domestic turkey (*Meleagris gallopavo*) and other galliform birds. *Zoology* **111**, 1095–1113 (2008).
60. Maxwell, E. E. Ossification sequence of the avian order Anseriformes, with comparison to other precocial birds. *J. Morphol.* **269**, 1095–1113 (2008).
61. Maxwell, E. E. & Harrison, L. B. Ossification sequence of the common tern (*Sterna hirundo*) and its implications for the interrelationships of the Lari (Aves, Charadriiformes). *J. Morphol.* **269**, 1056–1072 (2008).
62. Maxwell, E. E. & Larsson, H. C. E. Comparative ossification sequence and skeletal development of the postcranium of palaeognathous birds (Aves: Palaeognathae). *Zool. J. Linnean Soc.* **157**, 169–196 (2009).
63. Ikeda, T. et al. Distinct roles of Sox5, Sox6, and Sox9 in different stages of chondrogenic differentiation. *J. Bone Mineral Metab.* **23**, 337–340 (2005).
64. Lefebvre, V., Behringer, R. R. & de Crombrugghe, B. L-Sox5, Sox6 and Sox9 control essential steps of the chondrocyte differentiation pathway. *Osteoarthritis Cartilage* **9**, S69–S75 (2001).
65. Smits, P. et al. The transcription factors L-Sox5 and Sox6 are essential for cartilage formation. *Dev. Cell* **1**, 277–290 (2001).
66. Cancedda, R., Castagnola, P., Cancedda, F. D., Dozin, B. & Quarto, R. Developmental control of chondrogenesis and osteogenesis. *Int. J. Dev. Biol.* **44**, 707–714 (2000).
67. Eames, B. F., De La Fuente, L. & Helms, J. A. Molecular ontogeny of the skeleton. *Birth Defects Res. C* **69**, 93–101 (2003).
68. Miller, E. J. & Matukas, V. J. Chick cartilage collagen: a new type of α1 chain not present in bone or skin of the species. *Proc. Natl Acad. Sci. USA* **64**, 1264–1268 (1969).
69. Zhang, G., Eames, B. F. & Cohn, M. J. Evolution of vertebrate cartilage development. *Curr. Topics Dev. Biol.* **86**, 15–42 (2009).
70. Ninomiya, Y., Showalter, A. & Olsen, B. in *The Role of Extracellular Matrix in Development* (ed. Trelstad, R. L.) 255–275 (Alan R. Liss, 1984).
71. Botelho, J. F., Smith-Paredes, D., Nuñez-Leon, D., Soto-Acuña, S. & Vargas, A. O. The developmental origin of zygodactyl feet and its possible loss in the evolution of Passeriformes. *Proc. R. Soc. B* **281**, 20140765 (2014).
72. Botelho, J. F. et al. Skeletal plasticity in response to embryonic muscular activity underlies the development and evolution of the perching digit of birds. *Sci. Rep.* **5**, 09840 (2015).
73. Huh, J. W., Laurer, H. L., Raghupathi, R., Helfaer, M. A. & Saatman, K. E. Rapid loss and partial recovery of neurofilament immunostaining following focal brain injury in mice. *Exp. Neurol.* **175**, 198–208 (2002).
74. Schindelin, J. et al. Fiji: an open-source platform for biological-image analysis. *Nat. Methods* **9**, 676–682 (2012).
75. Schneider, C. A., Rasband, W. S. & Eliceiri, K. W. NIH Image to ImageJ: 25 years of image analysis. *Nat. Methods* **9**, 671–675 (2012).
76. Bookstein, F. L. *Morphometric Tools for Landmark Data: Geometry and Biology* (Cambridge University Press, 1997).
77. R Core Team. *R: A Language and Environment for Statistical Computing* (R Foundation for Statistical Computing, 2019).
78. Geomorph: software for geometric morphometric analyses (R package version 3.2.1) (2020).
79. Rohlf, F. J. The TPS series of software. *Hystrix* **26**, 9–12 (2015).
80. Charrad, M., Ghazzali, N., Boiteau, V. & Niknafs, A. NbClust: an R package for determining the relevant number of clusters in a data set. *J. Stat. Softw.* **61**, 1–36 (2014).
81. Buser, T. J., Sidlauskas, B. L. & Summers, A. P. 2D or not 2D? Testing the utility of 2D vs. 3D landmark data in geometric morphometrics of the sculpin subfamily Oligocottinae (Pisces; Cottoidea). *Anat. Rec.* **301**, 806–818 (2018).
82. Oksanen, J. et al. vegan: community ecology package (R package version 2.5-7). https://CRAN.R-project.org/package=vegan (2020).
83. Adams, D. C., Rohlf, F. J. & Slice, D. E. A field comes of age: geometric morphometrics in the 21st century. *Hystrix* **24**, 7–14 (2013).
84. Theska, T., Sieriebriennikov, B., Wighard, S. S., Werner, M. S. & Sommer, R. J. Geometric morphometrics of microscopic animals as exemplified by model nematodes. *Nat. Protoc.* **15**, 2611–2644 (2020).
85. Goodall, C. Procrustes methods in the statistical analysis of shape. *J. R. Stat. Soc. B* **53**, 285–339 (1991).
86. Drake, A. G. & Klingenberg, C. P. The pace of morphological change: historical transformation of skull shape in St Bernard dogs. *Proc. Biol. Sci.* **275**, 71–76 (2008).
87. Friendly, M. HE plots for repeated measures designs. *J. Stat. Softw.* **37**, 1–40 (2010).
88. Agnolin, F. L., Motta, M. J., Brissón Egli, F., Lo Coco, G. & Novas, F. E. Paravian phylogeny and the dinosaur–bird transition: an overview. *Front. Earth Sci.* **6**, 252 (2019).
89. Erickson, G. M. et al. Insights into the ecology and evolutionary success of crocodilians revealed through bite-force and tooth-pressure experimentation. *PLoS ONE* **7**, e31781 (2012).
90. Ezcurra, M. D. The phylogenetic relationships of basal archosauromorphs, with an emphasis on the systematics of proterosuchian archosauriforms. *PeerJ* **4**, e1778 (2016).
91. Nesbitt, S. J. The early evolution of archosaurs: relationships and the origin of major clades. *Bull. Am. Museum Nat. Hist.* **352**, 1–292 (2011).
92. Nesbitt, S. J. et al. A mid-Cretaceous tyrannosauroid and the origin of North American end-Cretaceous dinosaur assemblages. *Nat. Ecol. Evol.* **3**, 892–899 (2019).
93. Pritchard, A. C. & Sues, H.-D. Postcranial remains of *Teraterpeton hrynewichorum* (Reptilia: Archosauromorpha) and the mosaic evolution of the saurian postcranial skeleton. *J. Syst. Paleontol.* **17**, 1745–1765 (2019).
94. Rauhut, O. W. M., Hübner, T. R. & Lanser, K.-P. A new megalosaurid theropod dinosaur from the late Middle Jurassic (Callovian) of north-western Germany: implications for theropod evolution and faunal turnover in the Jurassic. *Palaeontologia Electronica* **19**, 29A (2016).
95. Cau, A. The assembly of the avian body plan: a 160-million-year long process. *Boll. Soc. Paleontol. Ital.* **57**, 1–25 (2018).
96. Cau, A., Brougham, T. & Naish, D. The phylogenetic affinities of the bizarre Late Cretaceous Romanian theropod *Balaur bondoc* (Dinosauria, Maniraptora): dromaeosaurid or flightless bird? *PeerJ* **3**, e1032 (2015).

97. Perrin, A. Recherches sur les affinités zoologiques de l'*Hatteria punctata*. *Ann. Sci. Nat.* **20**, 33–102 (1895).
98. Osawa, G. Beitrage zur Anatomie der *Hatteria punctata*. *Arch. Mikrosk. Anat.* **51**, 48–691 (1898).
99. Gregory, W. K. & Camp, C. L. Studies in comparative myology and osteology III. *Bull. Am. Museum Nat. Hist.* **38**, 447–563 (1918).
100. Byerly, T. The myology of *Sphenodon puncatum*. *Univ. Iowa Stud. Nat. Hist.* **11**, 3–51 (1925).
101. Walker, A. D. in *Problems in Vertebrate Evolution* (eds Andrews, S. M. et al.) 319–358 (Linnean Society, 1977).
102. Rowe, T. B. Homology and evolution of the deep dorsal thigh musculature in birds and other reptilia. *J. Morphol.* **189**, 327–346 (1986).
103. Dilkes, D. W. Appendicular myology of the hadrosaurian dinosaur *Maiasaura peeblesorum* from the Late Cretaceous (Campanian) of Montana. *Trans. R. Soc. Edin.* **90**, 87–125 (1999).
104. Carrano, M. T. & Hutchinson, J. R. Pelvic and hindlimb musculature of *Tyrannosaurus rex* (Dinosauria: Theropoda). *J. Morphol.* **253**, 207–228 (2002).
105. Allen, V. et al. Comparative architectural properties of limb muscles in Crocodylidae and Alligatoridae and their relevance to divergent use of asymmetrical gaits in extant Crocodylia. *J. Anat.* **225**, 569–582 (2014).
106. Klinkhamer, A. J., Wilhite, D. R., White, M. A. & Wroe, S. Digital dissection and three-dimensional interactive models of limb musculature in the Australian estuarine crocodile (*Crocodylus porosus*). *PLoS ONE* **12**, e0175079 (2017).
107. George, J. C. & Berger, A. J. *Avian Myology* (Academic Press, 1966).
108. Vanden Berge, J. C. & Zweers, G. A. in *Handbook of Avian Anatomy: Nomina Anatomica Avium* (eds Baumel, J. J. et al.) 189–250 (Publications of the Nuttall Ornithological Club 23, 1993).
109. Wellnhofer, P. *Archaeopteryx: The Icon of Evolution* (Verlag Dr. Friedrich Pfeil, 2009).
110. Padian, K. & Chiappe, L. M. The origin of birds and their flight. *Sci. Am.* **278**, 38–47 (1998).
111. Xu, X., You, H., Du, K. & Han, F. An *Archaeopteryx*-like theropod from China and the origin of Avialae. *Nature* **475**, 465–470 (2011).
112. Demuth, O. E., Rayfield, E. J. & Hutchinson, J. R. 3D hindlimb joint mobility of the stem-archosaur *Euparkeria capensis* with implications for postural evolution within Archosauria. *Sci. Rep.* **10**, 15357 (2020).
113. Gilmore, C. W. Osteology of the carnivorous Dinosauria in the United States National Museum, with special reference to the genera *Antrodemus* (*Allosaurus*) and *Ceratosaurus*. *Bull. US Natl Museum* **110**, 1–159 (1920).
114. Barsbold, R., Osmólska, H., Watabe, M., Currie, P. J. & Tsogtbaatar, K. A new oviraptorosaur (Dinosauria, Theropoda) from Mongolia: the first dinosaur with a pygostyle. *Acta Palaeontol. Polonica* **45**, 97–106 (2000).
115. Sullivan, R. M., Jasinski, S. E. & Van Tomme, M. P. A. A new caenagnathid *Ojoraptorsaurus boerei*, n. gen., n. sp. (Dinosauria, Oviraptorosauria), from the Upper Ojo Alamo Formation (Naashoibito Member), San Juan Basin, New Mexico. *New Mexico Museum Nat. Hist. Sci. Bull.* **53**, 418–428 (2011).
116. Kardon, G. Muscle and tendon morphogenesis in the avian hind limb. *Development* **125**, 4019–4032 (1998).
117. Alberch, P., Gould, S. J., Oster, G. F. & Wake, D. B. Size and shape in ontogeny and phylogeny. *Paleobiology* **5**, 296–317 (1979).
118. Romer, A. S. The development of tetrapod limb musculature—the thigh of *Lacerta*. *J. Morphol.* **71**, 251–298 (1942).

Acknowledgements We thank the Rockefeller Wildlife Refuge for *Alligator* eggs. Discussions with B. Wynd on ordination methods and variance–covariance matrices benefitted the final manuscript. We thank B. Pohl and the Wyoming Dinosaur Center for access to the Thermopolis specimen of *Archaeopteryx*, E. Updike and the Lawrence Livermore National Laboratory for laminography, J. Molnar for segmentation, D. Schwarz for access to the Berlin specimen, and A. Kirk and A. Baines for providing macrophotogrammetry. J.A. Gauthier provided useful comments and feedback throughout. M. Fox provided support for mounting and CT scanning at Yale. The Virginia Tech Paleobiology Research Group and H. Ueda provided discussion, and M. Stocker and S. Xiao gave feedback on earlier versions of the manuscript. C. Gordon provided feedback on the modularity discussion. M. Faunes and M. Cereghino provided assistance and feedback on the CLARITY protocol and segmentation. J. Nikolaus provided assistance with confocal microscopy. R. Diogo provided valuable feedback on earlier versions of this study. C.T.G. and R.M.C. were supported by National Science Foundation Graduate Research Fellowships. C.T.G. was supported by a National Science Foundation Postdoctoral Research Fellowship in Biology. R.M.C. was supported by National Science Foundation grant EAR-0917538 and software donations from FEI and Capturing Reality.

Author contributions C.T.G., J.F.B. and B.-A.S.B. designed the project. C.T.G., J.F.B. and B.-A.S.B. conceived and designed the experiments. C.T.G., J.F.B., M.H. and M.F. conducted experiments, and C.T.G. conducted analyses. S.M.G. assisted in planning of analyses and interpretation of data. C.T.G., J.F.B., M.H., M.F., R.M.C., M.A.N., S.E., D.-S.P., R.M.E., T.B.R., S.J.N. and B.-A.S.B. contributed material and/or material information. C.T.G. and B.-A.S.B. planned and wrote the manuscript with input from all authors.

Competing interests The authors declare no competing interests.

Additional information

Supplementary information The online version contains supplementary material available at https://doi.org/10.1038/s41586-022-04982-w.

Correspondence and requests for materials should be addressed to Bhart-Anjan S. Bhullar.

Peer review information *Nature* thanks Rui Diogo and the other, anonymous, reviewer(s) for their contribution to the peer review of this work.

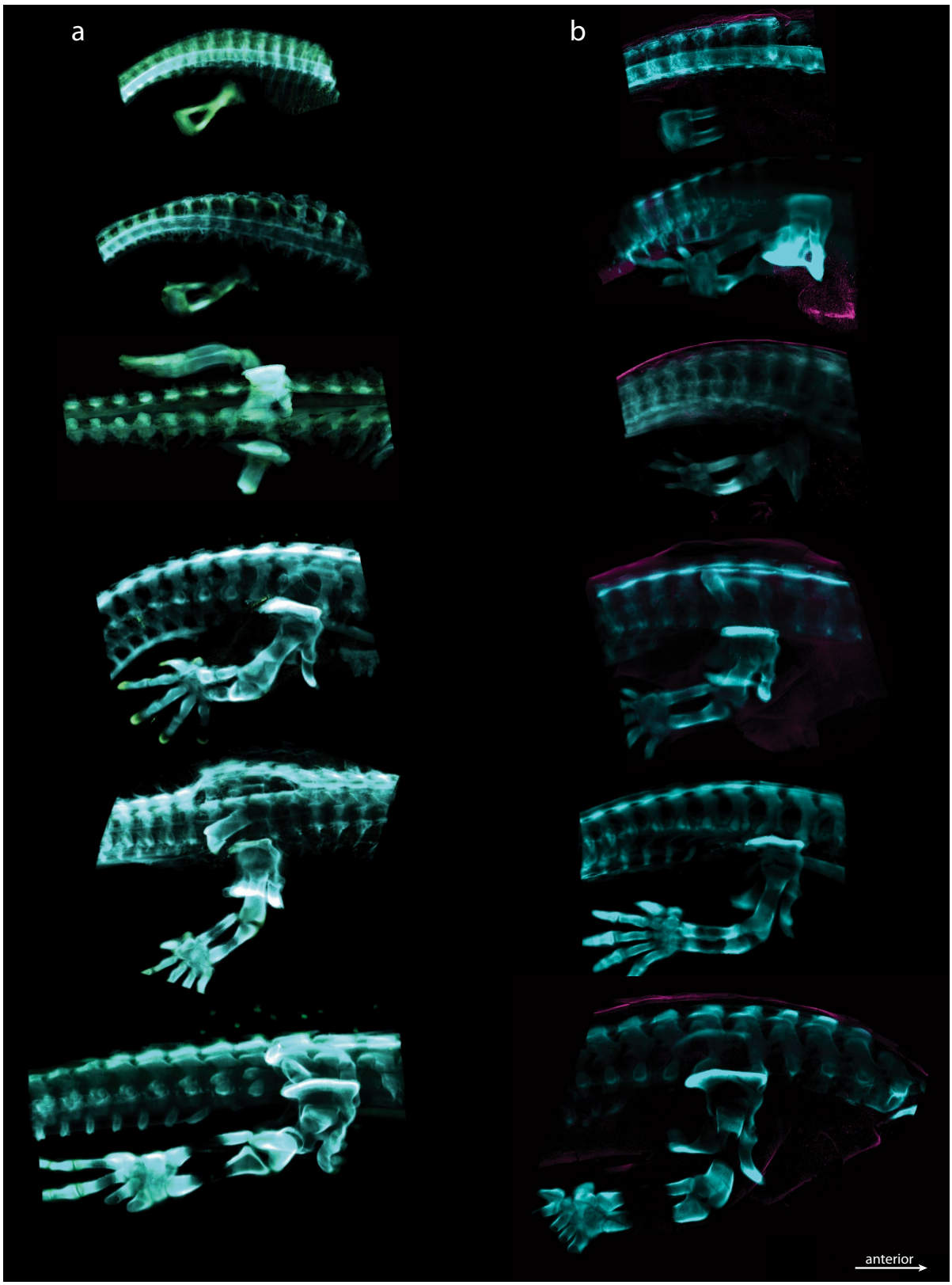

Extended Data Fig. 1 | Growth series of *Alligator mississippiensis* embryonic pelvis, hindlimb and tail stained for cartilage and connective tissue. **A**. Cartilage precursor and early cartilage (SOX-9, green) and cartilage (collagen II, blue). Approximate embryonic stages, top to bottom: F13 (15 days), F14 (16–17 days), F15 (18–20 days), F17 (22–23 days), F18 (25–26 days), F19 (27–28 days). **B**. Cartilage (collagen II, blue) and connective tissue (collagen I, purple). Approximate embryonic stages, top to bottom: F13 (15 days), F14 (16–17 days), F15 (18–20 days), F16 (21 days), F17 (22–23 days), F19 (27–28 days). [2 columns].

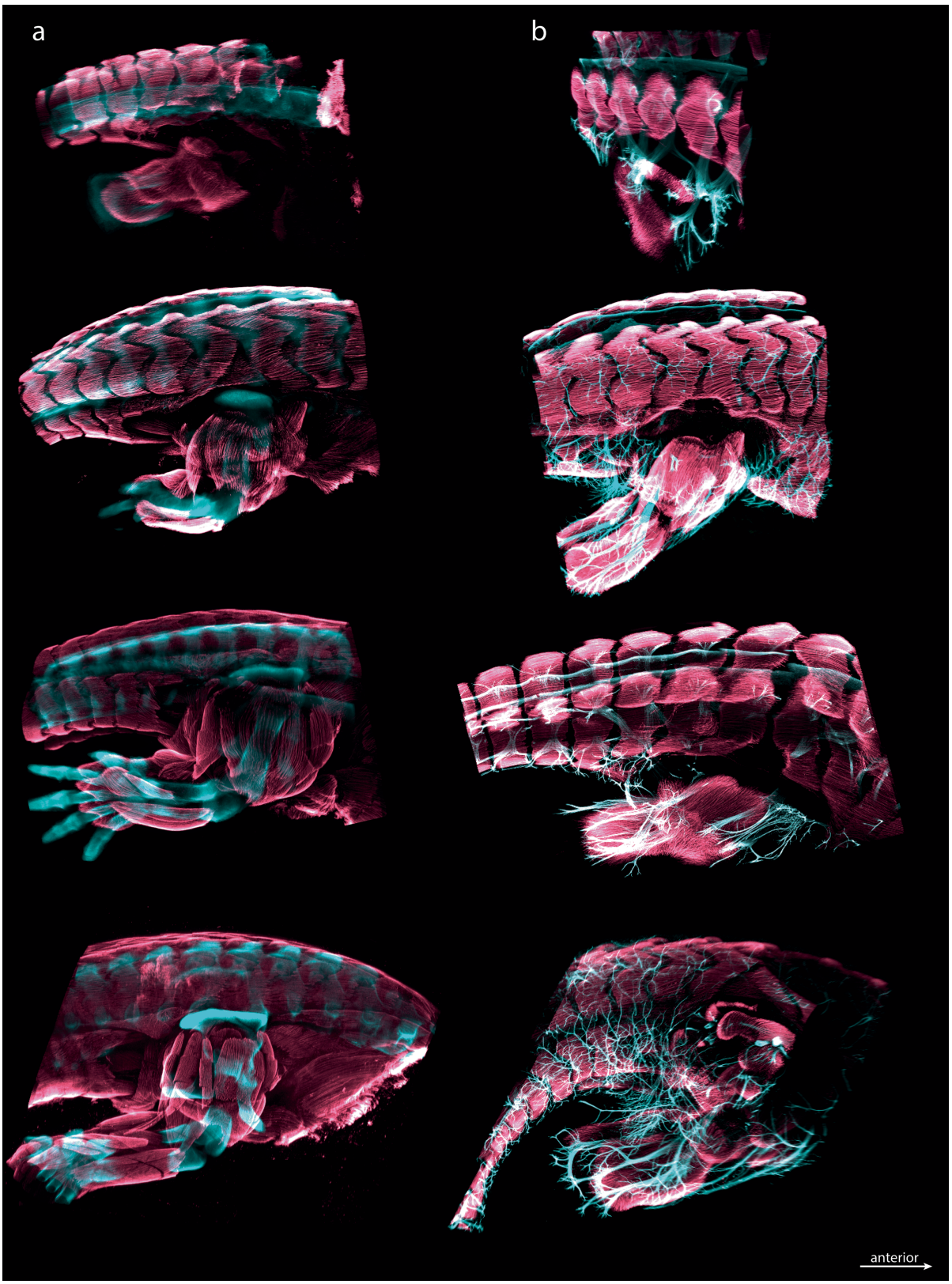

Extended Data Fig. 2 | Growth series of *Alligator mississippiensis* embryonic pelvis, hindlimb and tail stained for skeletal muscles, cartilage and nervous tissues. A. Cartilage (collagen II, blue) and skeletal muscle (MF-20, red). Approximate embryonic stages, top to bottom: F13 (15 days), F16 (21 days), F17 (22–23 days), F19 (27–28 days). **B**. Skeletal muscle (MF-20, red) and nervous tissue (NF-M, blue). Approximate embryonic stages, top to bottom: F13 (15 days), F15 (18–20 days), F16 (21 days), F17 (22–23 days). [2 columns].

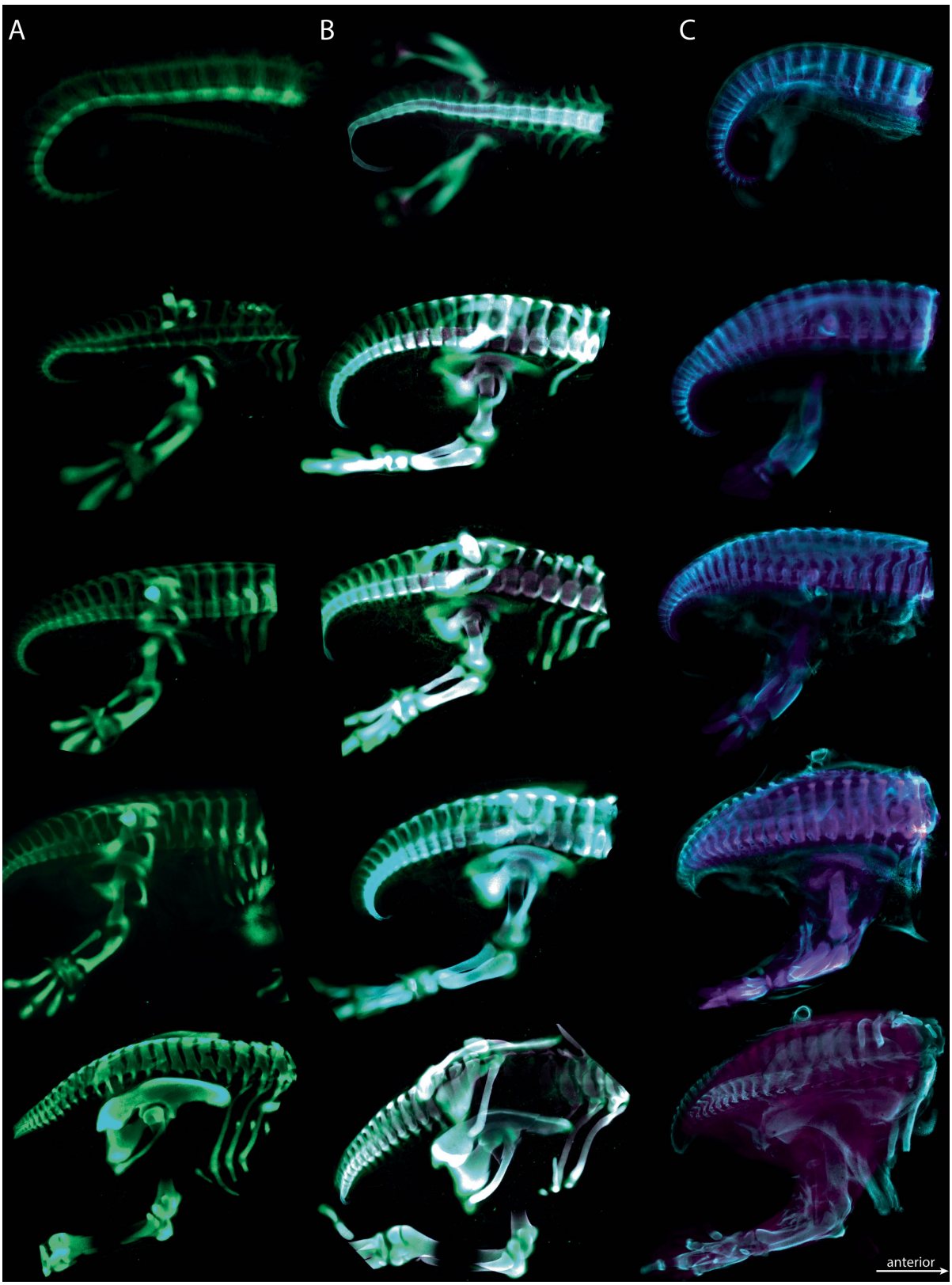

Extended Data Fig. 3 | Growth series of *Coturnix coturnix japonica* embryonic pelvis, hindlimb and tail stained for cartilage and connective tissue. A. Cartilage precursor and early cartilage (SOX-9, green). Approximate embryonic stages, top to bottom: HH24 (4 days of development), HH28 (5.5 days), HH29–30 (5.5–6.5 days), HH30 (6–6.5 days), HH34 (7.5 days). **B**. Cartilage precursor and early cartilage (SOX-9) and cartilage (collagen II, blue; collagen IX, purple). Approximate embryonic stages, top to bottom: HH27 (5 days), HH29 (5.5–6 days), HH30 (6–6.5 days), HH31 (6.5 days), HH34 (7.5 days). **C**. Connective tissue (tenascin, blue; collagen I, purple). Approximate embryonic stages, top to bottom: HH24 (4 days), HH27 (5 days), HH29 (5.5–6 days), HH30 (6–6.5 days), HH32 (7 days). [2 columns].

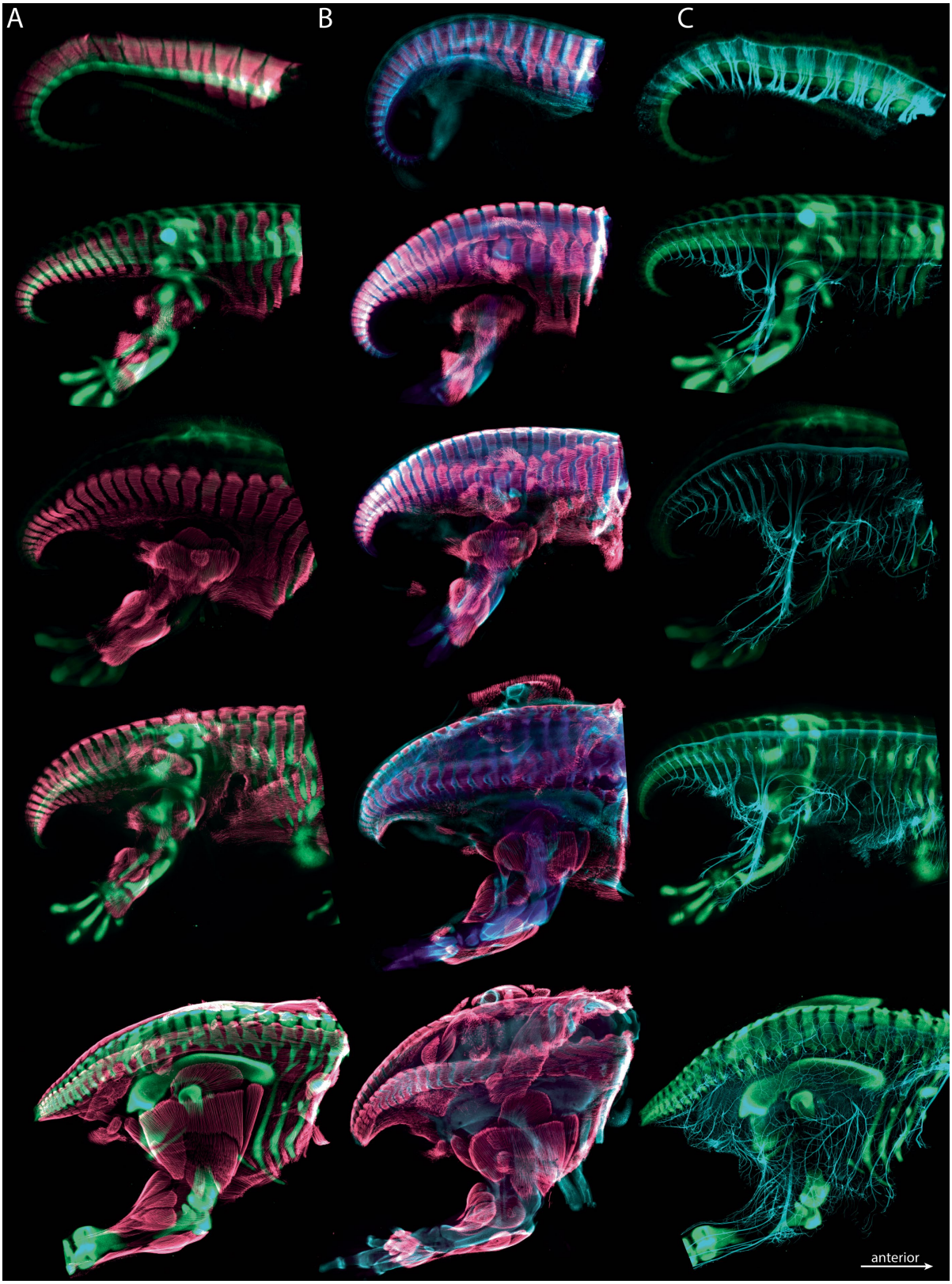

Extended Data Fig. 4 | Growth series of *Coturnix coturnix japonica* embryonic pelvis, hindlimb and tail stained for skeletal muscle, cartilage, connective tissue, and nervous tissue. A. Skeletal muscle (MF-20; red) and cartilage precursor and early cartilage (SOX-9, green). Approximate embryonic stages, top to bottom: HH24 (4 days), HH28–29 (5.5–6 days), HH29 (5.5–6 days), HH30 (6–6.5 days) HH34 (7.5 days). **B.** Skeletal muscle (MF-20, red) and connective tissue (tenascin, blue; collagen I, purple). Approximate embryonic stages, top to bottom: HH24 (4 days), HH27 (5 days), HH29 (5.5–6 days), HH30 (6–6.5 days), HH32 (7 days). C. Nervous tissue (NF-M, blue) and cartilage precursor and early cartilage (SOX-9, green). Approximate embryonic stages, top to bottom: HH24 (4 days), HH28–29 (5.5–6 days), HH29 (5.5–6 days), HH30 (6–6.5 days) HH34 (7.5 days). [2 columns].

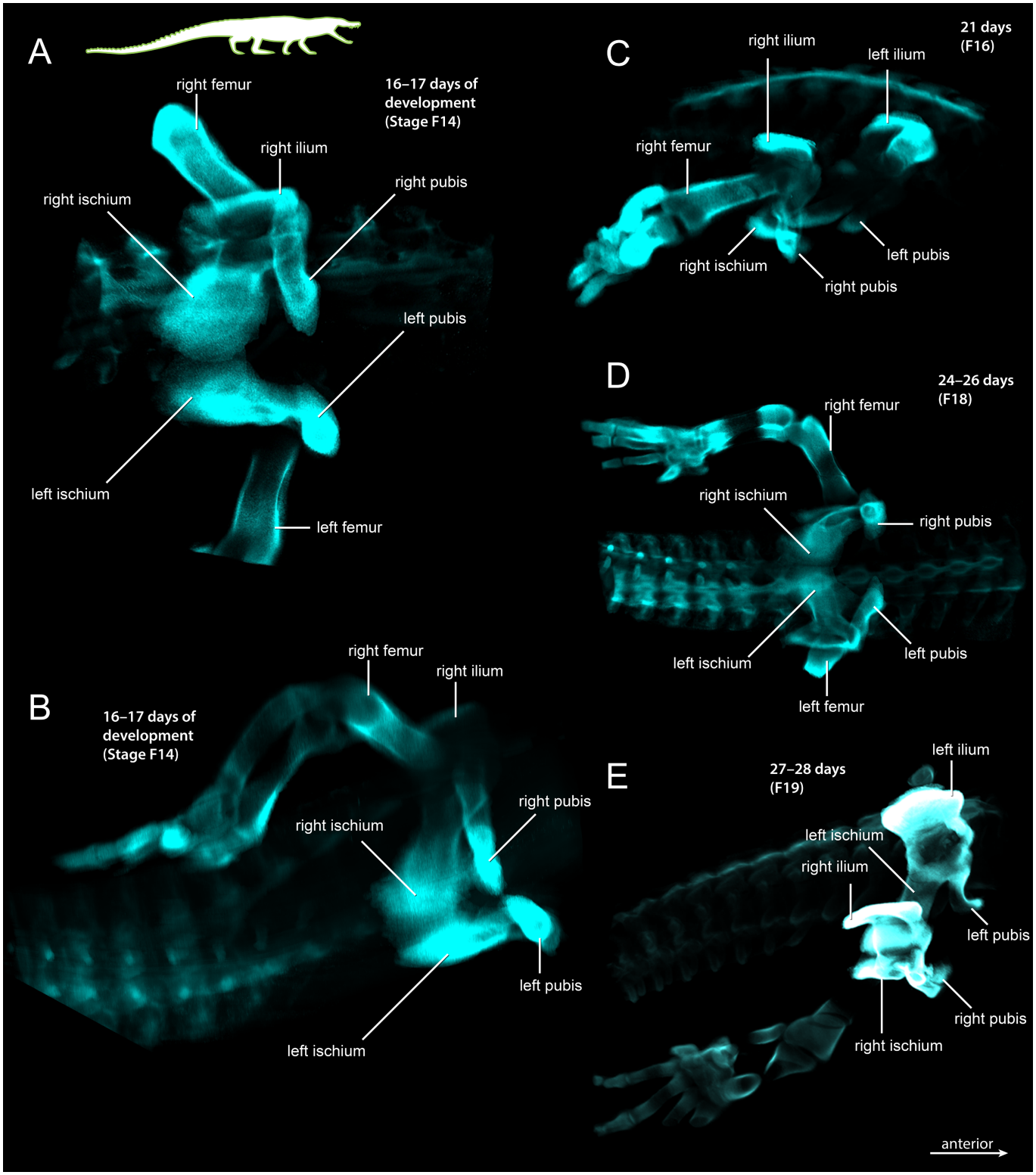

Extended Data Fig. 5 | The distal ends of the pubis in *Alligator mississippiensis* remain unfused during early organogenesis of the pelvis. A. Stage F14 (16–17 days of development) pelvis in right ventrolateral view (reversed). B. Stage F14 pelvis in right oblique ventrolateral view. C. Stage 16 (21 days) pelvis in right oblique anterolateral view. D. Stage 18 (24–26 days) pelvis ventral view. E. Stage 19 (27–28 days) pelvis in right anterolateral view. Blue stains are collagen II. [2 columns].

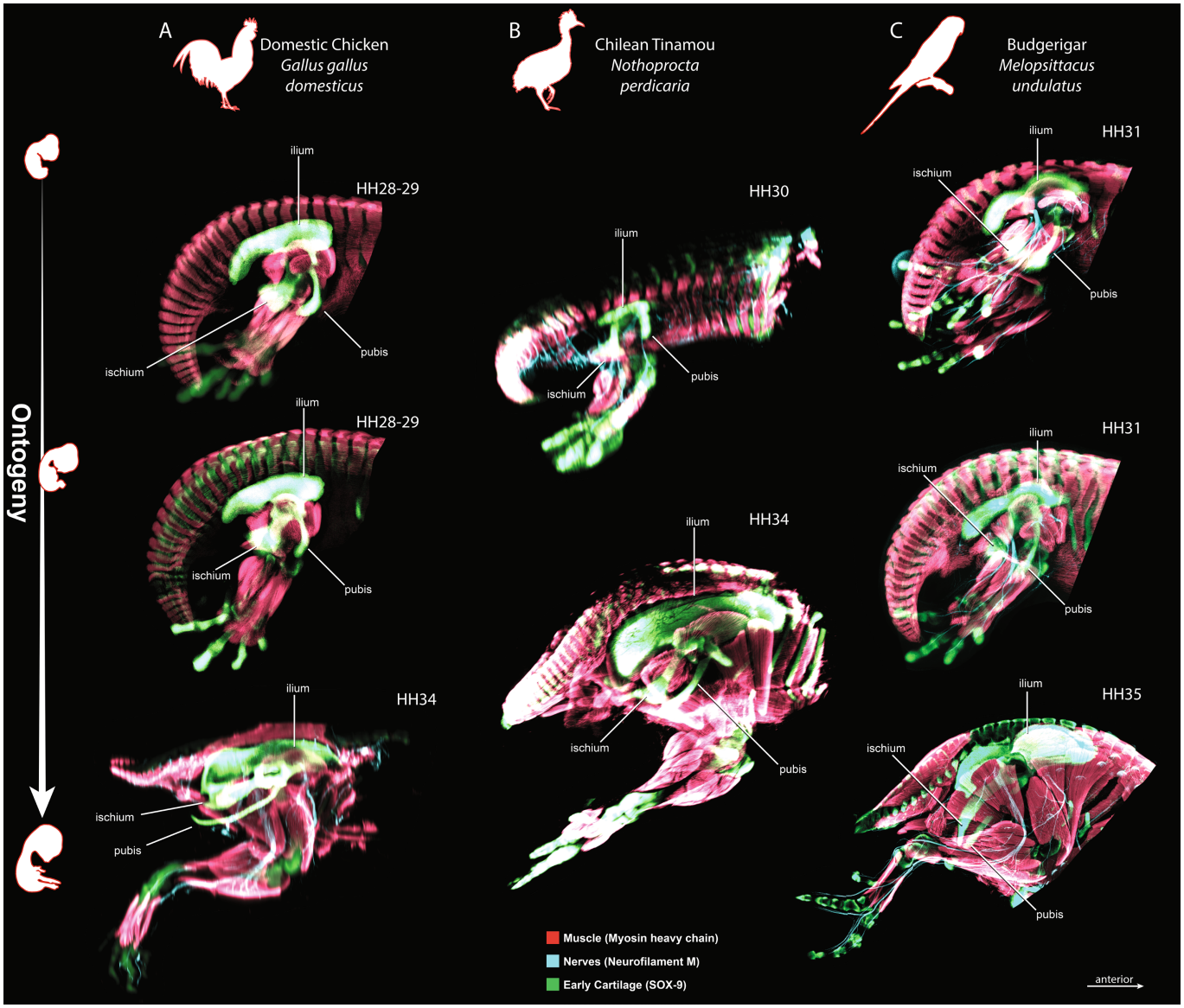

Extended Data Fig. 6 | Embryological series of other avian taxa stained for cartilage precursor and early cartilage (SOX-9), skeletal muscle (MF-20), and nervous tissue (NF-M). Note that the ancestral states described in *Coturnix* development (e.g., anteriorly short ilium, non-retroverted pubis, pubic 'boot') appear in early organogenetic stages of these taxa as well. A. Growth series of the Domestic Chicken (*Gallus gallus domesticus*), a galloanseriform. Approximate embryonic stage, top to bottom: HH29, HH29, HH34. B. Growth series of the Chilean Tinamou (*Nothoprocta perdicaria*), a paleognath. Approximate embryonic stage, top to bottom: HH30, HH34. B. Growth series of the Budgerigar (*Melopsittacus undulatus*), a neoavian. Approximate embryonic stage, top to bottom: HH31 (early), HH31 (late), HH35. [2 columns].

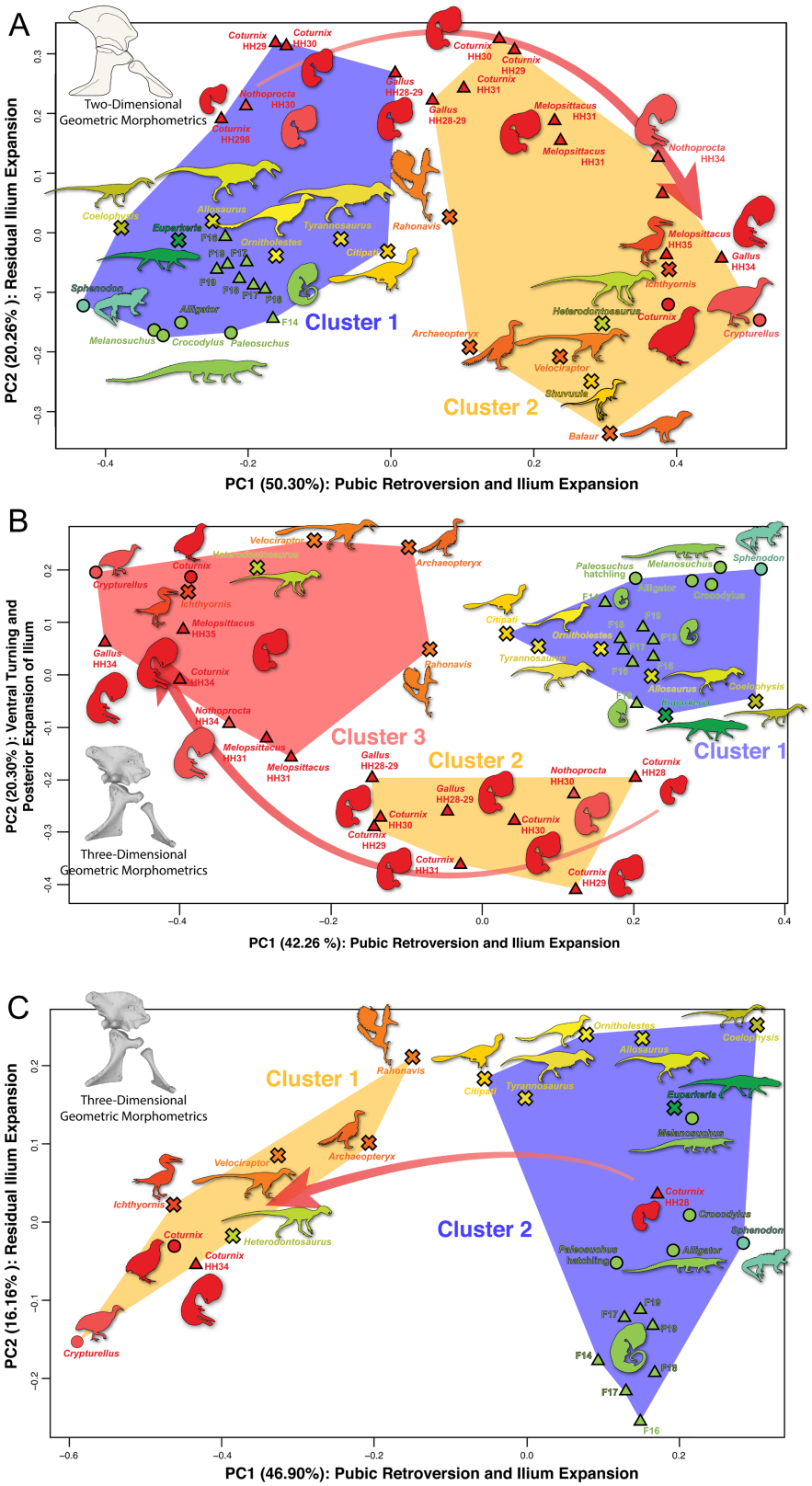

Extended Data Fig. 7 | Geometric morphometrics with results of cluster analyses. A. 2D geometric morphometrics with results of cluster analysis. Note that the PC1 axis is inverted for ease of comparison. **B**. 3D geometric morphometrics with results of cluster analysis. **C**. 3D geometric morphometrics with intermediate quail embryonic stages excluded from geometric morphometric analysis, with results of cluster analysis. [2 columns].

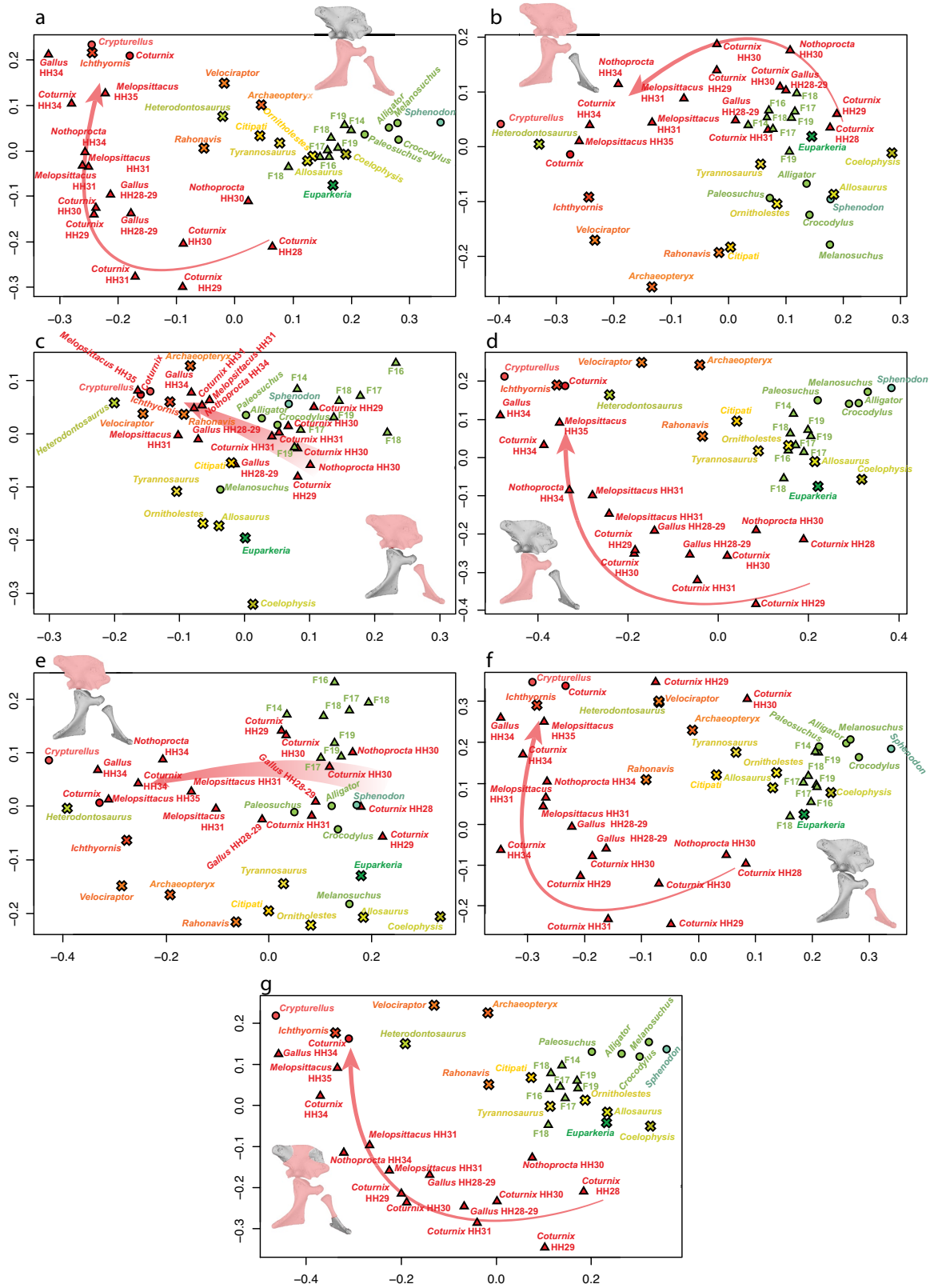

Extended Data Fig. 8 | Results of 3D geometric morphometrics performed on partitions of landmarks. A. Ilium landmarks (landmarks 1–5). **B**. Pubis landmarks (landmarks 6–9). **C**. Ischium landmarks (landmarks 10–13). **D**. Ilium and pubis landmarks (landmarks 1–9) **E**. Pubis and ischium landmarks (landmarks 6–13). **F**. Ilium and ischium landmarks (landmarks 1–5, 10–13). **G**. extremes of ilium and extremes of pubis landmarks (landmarks 1, 3, 7, 8). [2 columns].

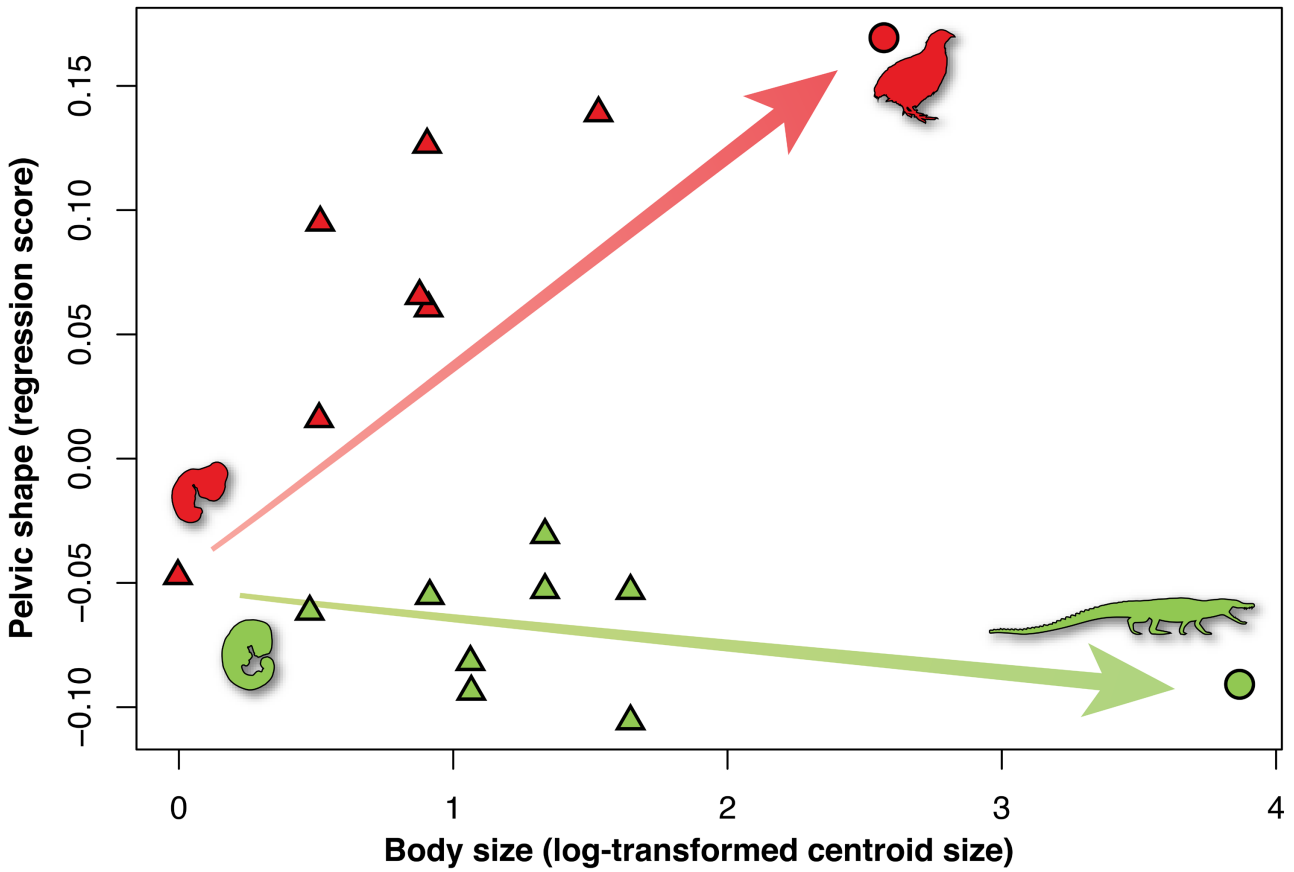

Extended Data Fig. 9 | Quantified ontogenetic allometric trajectories of *Coturnix* and *Alligator* pelvic development suggests that *Coturnix* ontogeny is characterized by heterochronic acceleration. Both trajectories start at similar shapes, but *Alligator* shape change during ontogeny is minimal, whereas *Coturnix* pelvic shape changes greatly with a steep slope. This suggests that acceleration is present in avian pelvic ontogeny, as is expected for terminal addition[117]. The differing ontogenetic trajectories of *Coturnix* and *Alligator* suggests that the avian pelvis did not evolve via peramorphosis. This is supported by the observation that the *Alligator* pubis slightly proverts and the ilium becomes proportionally taller during ontogeny (Figs. 2, 4), as well as descriptions of *Lacerta* ontogeny indicating a similar conservatism in developmental trajectory[118]. [1 column].

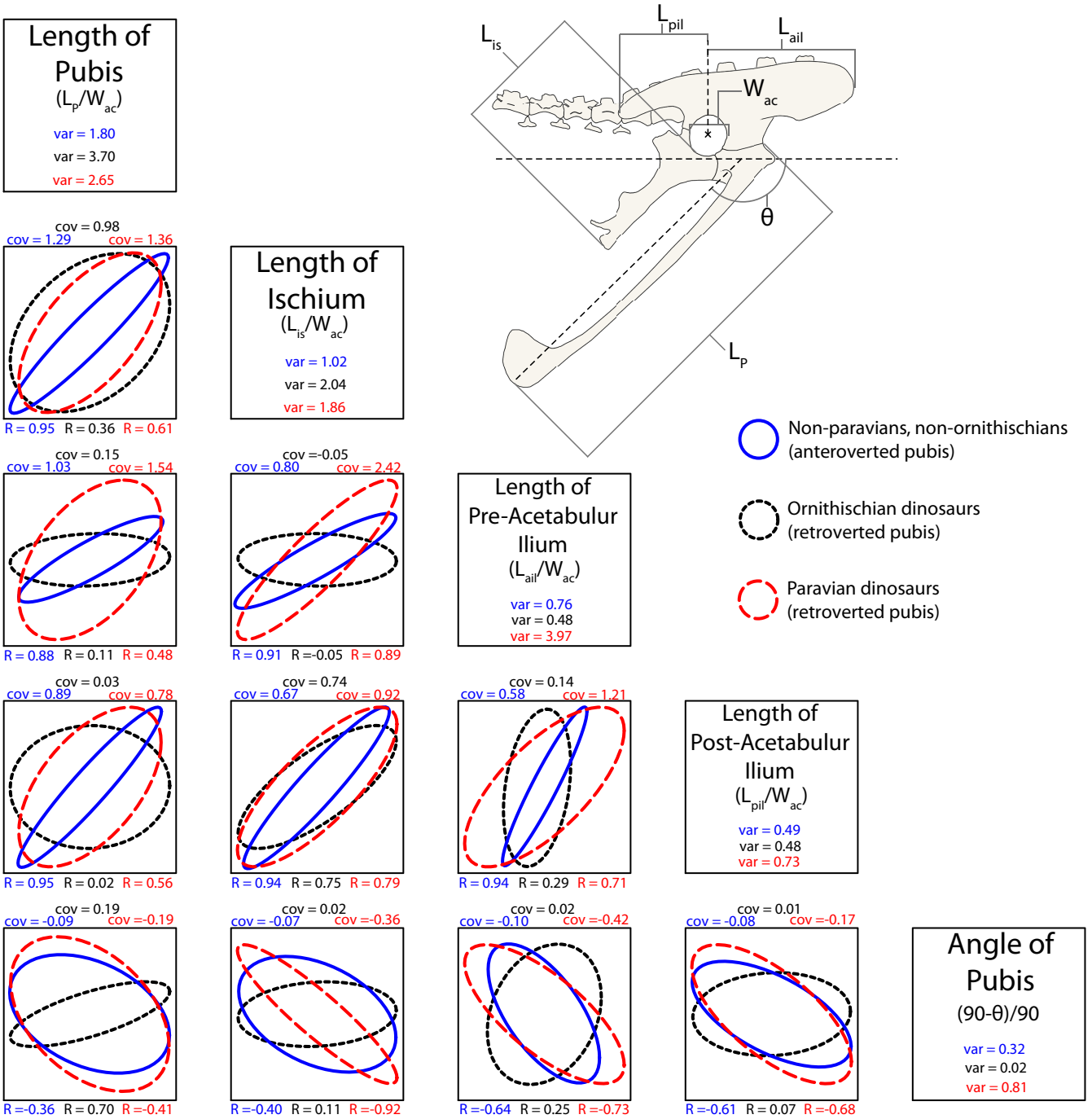

Extended Data Fig. 10 | Variance-covariance plots for paravians, other archosaurs, and ornithischians. Note that paravians and other archosaurs are nearly identical, especially in direction, and ornithischians are often divergent. The pelvis does not depict a specific taxon, but illustrates how proportions and angles were measured. [2 columns].

nature portfolio

Corresponding author(s): Bhart-Anjan S. Bhullar

Last updated by author(s): Jun 1, 2022

Reporting Summary

Nature Portfolio wishes to improve the reproducibility of the work that we publish. This form provides structure for consistency and transparency in reporting. For further information on Nature Portfolio policies, see our Editorial Policies and the Editorial Policy Checklist.

Statistics

For all statistical analyses, confirm that the following items are present in the figure legend, table legend, main text, or Methods section.

n/a	Confirmed	
☐	☒	The exact sample size (*n*) for each experimental group/condition, given as a discrete number and unit of measurement
☐	☒	A statement on whether measurements were taken from distinct samples or whether the same sample was measured repeatedly
☐	☒	The statistical test(s) used AND whether they are one- or two-sided *Only common tests should be described solely by name; describe more complex techniques in the Methods section.*
☐	☒	A description of all covariates tested
☐	☒	A description of any assumptions or corrections, such as tests of normality and adjustment for multiple comparisons
☐	☒	A full description of the statistical parameters including central tendency (e.g. means) or other basic estimates (e.g. regression coefficient) AND variation (e.g. standard deviation) or associated estimates of uncertainty (e.g. confidence intervals)
☐	☒	For null hypothesis testing, the test statistic (e.g. *F*, *t*, *r*) with confidence intervals, effect sizes, degrees of freedom and *P* value noted *Give P values as exact values whenever suitable.*
☒	☐	For Bayesian analysis, information on the choice of priors and Markov chain Monte Carlo settings
☒	☐	For hierarchical and complex designs, identification of the appropriate level for tests and full reporting of outcomes
☐	☒	Estimates of effect sizes (e.g. Cohen's *d*, Pearson's *r*), indicating how they were calculated

Our web collection on statistics for biologists contains articles on many of the points above.

Software and code

Policy information about availability of computer code

Data collection	Landmark software (v. 3.0.0.6), ImageJ/Fiji
Data analysis	R75 package geomorph76 (v. 3.2.1), VGStudio MAX 3.3, R package NbClust, R package vegan

For manuscripts utilizing custom algorithms or software that are central to the research but not yet described in published literature, software must be made available to editors and reviewers. We strongly encourage code deposition in a community repository (e.g. GitHub). See the Nature Portfolio guidelines for submitting code & software for further information.

Data

Policy information about availability of data

All manuscripts must include a data availability statement. This statement should provide the following information, where applicable:

- Accession codes, unique identifiers, or web links for publicly available datasets
- A description of any restrictions on data availability
- For clinical datasets or third party data, please ensure that the statement adheres to our policy

All data files used for analyses, and all code, are hosted on DRYAD (https://doi.org/10.5061/dryad.xd2547dj2). All fossils are reposited in recognized natural history institutions.

Human research participants

Policy information about studies involving human research participants and Sex and Gender in Research.

Reporting on sex and gender	N/A
Population characteristics	N/A
Recruitment	N/A
Ethics oversight	N/A

Note that full information on the approval of the study protocol must also be provided in the manuscript.

Field-specific reporting

Please select the one below that is the best fit for your research. If you are not sure, read the appropriate sections before making your selection.

☐ Life sciences ☐ Behavioural & social sciences ☒ Ecological, evolutionary & environmental sciences

For a reference copy of the document with all sections, see nature.com/documents/nr-reporting-summary-flat.pdf

Ecological, evolutionary & environmental sciences study design

All studies must disclose on these points even when the disclosure is negative.

Study description	We performed a comparative analysis of embryonic development and evolutionary morphology of the reptilian pelvis.
Research sample	Research sample was a collection of previously obtained embryos and fossil specimens.
Sampling strategy	Sample selection of fossils was subject to availability. Sample sizes for embryonic development followed convention in the ontogeny/development literature.
Data collection	Data collection performed digitally by authors as specified, on three-dimensional datasets.
Timing and spatial scale	2015-2020, periodic work on image collection and datasets. Materials had already been collected.
Data exclusions	No exclusions.
Reproducibility	All methods thoroughly described and image data/code made available.
Randomization	N/A study was on ontogenetic anatomy and evolutionary morphology.
Blinding	N/A specimens already collected/identified.

Did the study involve field work? ☐ Yes ☒ No

Reporting for specific materials, systems and methods

We require information from authors about some types of materials, experimental systems and methods used in many studies. Here, indicate whether each material, system or method listed is relevant to your study. If you are not sure if a list item applies to your research, read the appropriate section before selecting a response.

Materials & experimental systems

n/a	Involved in the study
☒	☐ Antibodies
☒	☐ Eukaryotic cell lines
☐	☒ Palaeontology and archaeology
☒	☐ Animals and other organisms
☒	☐ Clinical data
☒	☐ Dual use research of concern

Methods

n/a	Involved in the study
☒	☐ ChIP-seq
☒	☐ Flow cytometry
☒	☐ MRI-based neuroimaging

Palaeontology and Archaeology

Specimen provenance	Museum specimens
Specimen deposition	Yale Peabody Museum of Natural History, American Museum of Natural History (see manuscript)
Dating methods	N/A

☐ Tick this box to confirm that the raw and calibrated dates are available in the paper or in Supplementary Information.

Ethics oversight	No approval required — existing specimens used.

Note that full information on the approval of the study protocol must also be provided in the manuscript.